Interpretation with the Europlexus code of the MARA8 experiment simulating a hypothetical Core Disruptive Accident

Marie-France Robbe, Michel Lepareux, Yves Cariou

INTERPRETATION WITH THE EUROPLEXUS CODE OF THE MARA8 EXPERIMENT SIMULATING A HYPOTHETICAL CORE DISRUPTIVE ACCIDENT

Keywords: explosion, safety, Fast Breeder Reactor

M.F. Robbe[1], M. Lepareux[1], Y. Cariou[2]

(1) CEA Saclay, SEMT-DYN, 91191 Gif sur Yvette cedex, France,
phone: (33) 1 69 08 87 49, e-mail: marie-france.robbe@cea.fr or mfrobbe@cea.fr
(2) Novatome, NVPM,10 rue Juliette Récamier, 69006 Lyon, France

ABSTRACT

In the case of a Hypothetical Core Disruptive Accident (HCDA) in a Liquid Metal Fast Breeder Reactor, it is assumed that the core of the nuclear reactor has melted partially and that the chemical interaction between molten fuel and liquid sodium has created a high-pressure gas bubble in the core. The violent expansion of this bubble loads and deforms the reactor vessel, thus endangering the safety of the nuclear plant. The experimental test MARA8 simulates the explosive phenomenon in a mock-up included in a flexible vessel with a flexible roof. This paper presents a numerical simulation of the test and a comparison of the computed results with the experimental results and previous numerical ones.

1 INTRODUCTION

To ensure a high safety level in French nuclear power plants, safety authorities require plant designers to take into consideration several cases of hypothetical severe accidents which the plant must be able to withstand. The aim is to guarantee that even a core-melt accident would not require any stringent countermeasures such as evacuation or relocation of the population beyond the immediate vicinity of the plant.

For the Liquid Metal Fast Breeder Reactors (LMFBR), one of the severe accidents envisaged is a Hypothetical Core Disruptive Accident (HCDA). The scenario supposes that the core of the reactor has melted partially due to an accident. The chemical interaction of molten fuel with the liquid sodium used to cool the reactor core very quickly produces a high quantity of gaseous components.

A high-pressure gas bubble forms in the core centre. The explosive expansion of this bubble leads to an overloading of the reactor vessel and its internal structures. To avoid the release of radioactive products in the plant containment, the integrity of the reactor vessel must be maintained.

During the 70s and 80s, several countries contributed to the understanding of the consequences of a HCDA. They undertook several experimental programmes or developed computer codes especially devoted to the analysis of the transient loads resulting from a HCDA. The codes generally aimed at simulating a HCDA in the reactor in order to demonstrate its capacity to withstand such an accident. The experimental programmes had more varied objectives.

The STROVA and COVA programmes were dedicated to the validation of the computer codes. The STROVA programme [17] consisted in applying well-defined transient loads to a variety of metal structures (representative of the reactor roof and the components of the reactor vessel) and in comparing the experimental results with those computed by the EURDYN structural dynamics code.

The COVA programme (COde VAlidation) [15] [14] [2] relied on a series of experiments performed in cylindrical tanks, starting with simple tests and increasing in complexity in such a way that only one new feature was introduced at a time. This programme aimed at validating [41] [16] the ASTARTE and SEURBNUK codes.

The WINCON and MARA programmes involved tests of gradual complexity which were based on small-scale replicas of reactors. The interest of the WINCON programme (WINfrith CONtainment) [38] was both to understand the influence of the presence of each internal structure in the global response of the reactor and to validate the SEUBNUK and EURDYN codes.

Based on a 1/30 scale model of the Superphenix reactor, the French programme MARA involved ten tests of gradual complexity due to the successive addition of internal deformable structures:
- MARA 1 and 2 considered a vessel partially filled with water and topped with a rigid roof [1],
- MARA 4 represented the main core support structures [39],
- MARA 8 and 9 used a flexible roof [12],
- MARA 10 included the core support structures and a simplified representation of the structures above the core [23].

The French SIRIUS code [4] [10] was validated on the MARA programme [24] [5]. Like other codes using a Lagrangian approach, SIRIUS required rezoning during calculation because the deformation of the internal structures caused a great distortion of the fluid meshes. Sodium and the thick structures (the roof) were described with the Finite Difference Method while the Finite Element Method was used for the thin structures (the vessel). Argon and the bubble were not meshed, but taken into account by a law computing volume versus pressure.

At the end of the 80s, it was preferred to add a specific HCDA sodium-bubble-argon tri-component constitutive law [20] to the general fast dynamics finite element CASTEM-PLEXUS code. The HCDA constitutive law was validated [8] by the CONT benchmark [3].

In order to demonstrate the capability of CASTEM-PLEXUS to predict the behaviour of real reactors [21] [7], axisymmetrical computations of the MARA series were confronted with the experimental results. The computations performed at the beginning of the 90s showed a rather good agreement between the experimental and computed results for the MARA 8 and MARA 10 tests [6]. However, numerical results showed some discrepancies which might be eliminated by increasing the fineness of the mesh. Afterwards, the CASTEM-PLEXUS code was merged with the PLEXIS-3C code to extend the capacities of both codes: the result was the EUROPLEXUS code.

At the end of the 90s, the mesh of the MARA 8 model was refined and a more detailed analysis of results was undertook [31] [34] [32] [35]. This simulation presented results in closer agreement with the MARA 8 test. In parallel, simulations of the MARA 10 were carried out with an improved fluid-structure coupling; they showed that the numerical results were better with this new coupling.

To conclude the MARA 8 test, we undertook recently another simulation with the fine mesh and the new fluid-structure coupling. In addition, owing to the increased possibilities of computers, it was possible to carry out the simulation for a longer period of physical time. After a brief presentation of the MARA 8 mock-up and of the EUROPLEXUS code, this paper focuses on the numerical model, the analysis of the numerical results and a comparison of the current numerical results with the experimental results and with the previously computed ones.

2 DESCRIPTION OF THE MARA8 MOCK-UP

In France, the two Liquid Metal Fast Breeder Reactors (LMFBR) Phenix and Superphenix (see Fig. 1) are based on an integrated design: the entire primary circuit of the reactor (core, pumps, heat exchangers, etc.) is included inside the reactor vessel. The exchanges with the secondary circuit are limited to some pipes crossing the reactor roof. The main advantage of this design is to maintain the majority of the radioactive elements inside the reactor vessel and to limit the possible contacts between air and the radioactive sodium of the primary circuit. As sodium is flammable on contact with air, a blanket of inert gas (argon) isolates the sodium in the reactor block from the reactor roof.

The MARA programme was defined and realised at the CEA-Cadarache in the 80s in order to simulate a Hypothetical Core Disruptive Accident in simplified small-scale models of the Superphenix reactor block. The characteristics of the MARA mock-ups were [6]:
- a scale factor of 1/30 for all dimensions and thicknesses,
- an axisymmetrical geometry.

In order to carry out tests at ambient temperature and to avoid fire problems linked to sodium handling, liquid sodium was replaced by water in tests since both components have similar densities and viscosities. Argon was replaced by air, and the bubble expansion was simulated by an explosive source.

All tests of the MARA series were fired using a 45 g low-density low-pressure explosive charge of L54/16 composition [11] leading to at least a 1000 MJ full-scale energy release [24]. Vessels were filled with water leaving a 4.3 cm air gap [12]. The vessels of all the tests were identical and made of 316 steel 1.2 mm thick. Between the junction with the core support plate and the junction with the internal heat exchangers, the thickness was reduced locally to 0.9 mm and 1.1 mm in order to simulate a pinned attachment with the diagrid.

In MARA8, a flexible roof of A42 steel 10 mm thick was clamped to the roof support [12]. The vessel was welded to a flange bolted to the roof support. The external dimensions of the MARA 8 mock-up were a height of 55 cm and a radius of 35 cm. The mock-up (see Fig. 2) did not include internal structures. The explosive charge was hung from the roof centre.

The mock-up was well instrumented [12] with:
• 7 pressure transducers fitted under the roof at different radii,
• 8 strain gauges placed on the upper and lower sides of the roof at three radial locations (centre, mid-radius and near the edge),
• 6 strain gauges attached at three main locations on the vessel (upper bulge, charge level and base) to obtain axial and hoop strains,
• 2 high-speed cameras used to obtain displacements of the roof and the vessel (upper bulge and base).
The residual deformations were evaluated by measuring, before and after the firing, the mesh sizes of the grid drawn on the vessel and the roof.

3 DESCRIPTION OF THE EUROPLEXUS COMPUTER CODE AND OF THE HCDA CONSTITUTIVE LAW

EUROPLEXUS is a general computer code [9] [13] [25], co-developed by CEA-Saclay and JRC-Ispra, for the analysis of fast transient phenomena. EUROPLEXUS results from the merging of the CASTEM-PLEXUS and PLEXIS-3C codes. It can perform 1D, 2D or 3D structure calculations as required. The main fields dealt with are impacts [27], explosions [26] [28] [29] [33] [36], pipe circuits [18] [19] [30] [37], hydrodynamics [40] and robots [22].

EUROPLEXUS is based on the Finite Element Method. Time integration is explicit and the formulation can be Lagrangian, Eulerian or Arbitrary Lagrange Euler (ALE). The code can take into account various non-linearities related to materials or geometry. EUROPLEXUS calculates successively, at each time step, the mass conservation, the total energy conservation only if needed, the material constitutive law and finally the momentum conservation law.

The HCDA constitutive law of the EUROPLEXUS code supposes that the sodium-argon-bubble mixture is homogeneous in each mesh. Each constituent is described by a specific law, and it is assumed that the presence of the other constituents does not affect the constitutive law of each one. Thermal transfers between constituents during the explosion are assumed to be negligible. As a consequence of this simplification, the code does not use the energy equation for the resolution of HCDA problems.

The mass conservation is ensured by balancing the flows crossing the mesh boundary during the time step. Then the code solves the weak formulation of the momentum equation:
Mass conservation $M^{(n+1)} = M^{(n)} + \Delta M^{(n \to n+1)}$
with

$$\Delta M^{(n \to n+1)} = - \int_{t^{(n)}}^{t^{(n+1)}} \oint_A \rho \, \vec{n}.\vec{v} \, dA \, dt + \int_{t^{(n)}}^{t^{(n+1)}} \int_V M_{ext} \, dV \, dt$$

Weak formulation of the momentum conservation

$$\underbrace{\int_{t^{(n)}}^{t^{(n+1)}} \int_V \vec{U}^*. \, \rho \frac{\partial \vec{v}}{\partial t} dV \, dt}_{M^{(n+1)} \gamma^{(n+1)}} + \underbrace{\int_{t^{(n)}}^{t^{(n+1)}} \int_V \vec{U}^*. \left(\rho \, \vec{v}.\bar{\bar{\epsilon}} \right) dV \, dt}_{\text{transport force}} - \underbrace{\int_{t^{(n)}}^{t^{(n+1)}} \oint_A \vec{n}. \left(\vec{U}^*.\bar{\bar{\sigma}} \right) dA \, dt}_{\text{boundary conditions}}$$

$$\underbrace{+\int_{T^{(n)}}^{T^{(n+1)}}\int_V \dot{\overline{\overline{\epsilon}}}^{*} : \overline{\overline{\sigma}}\, dV\, dt}_{\text{internal forces}} = \underbrace{\int_{T^{(n)}}^{T^{(n+1)}}\int_V \vec{F}_{ext}\, dV\, dt}_{\text{external forces}}$$

with

A	bounding surface	V	volume
$\vec{F}_{ext}$	external forces	$\vec{v}$	velocity
M	mass	$\vec{\gamma}$	acceleration
M_{ext}	external mass source	ρ	density
$\vec{n}$	normal vector	$\overline{\overline{\epsilon}}^{*}$	strain (spatial derivative of $\vec{U}^{*}$)
n	time step	$\dot{\overline{\overline{\epsilon}}}$	strain speed (spatial derivative of $\vec{v}$)
t	time	$\overline{\overline{\sigma}}$	stress
$\vec{U}^{*}$	arbitrary displacement		

In the Finite Element Model, the nodal variables (velocity, acceleration, etc.) are identical for the three constituents of the HCDA law. On the contrary, the elementary variables (pressure, density, etc.) depend on several parameters: the partial variables of each constituent, the presence fraction x of constituents, etc. The quantities related to each constituent (a for argon, b for bubble, s for sodium and v for sodium vapour) are indicated with a subscript. Quantities without subscript are related to the homogeneous mixture, and index g is related to the gas mixture.

For instance, the mixture density is obtained by:

$$\rho = \rho_a\, x_a + \rho_b\, x_b + \rho_s\, x_s + \rho_v\, x_v$$

The pressure of the gas mixture p_g is the sum of the partial pressures:

$$p_g^{(n+1)} = p_a^{(n+1)} + p_b^{(n+1)} + p_v^{(n+1)} \qquad (1)$$

The void fraction α is obtained from the ratios between the relative density ϕ of a component (density related to the total volume of the mesh) and the absolute density of the component:

$$\alpha = \frac{\phi_a}{\rho_a} = \frac{\phi_b}{\rho_b} = \frac{\phi_v}{\rho_v} = \frac{\phi_g}{\rho_g} = 1 - \frac{\phi_s}{\rho_s} \qquad (2)$$

The fluid mixture is described by the constitutive laws of each component [21].

• Argon is assumed to be a perfect gas with an adiabatic behaviour:

$$p_a^{(n+1)} = p_a^{(n)} \left(\frac{\rho_a^{(n+1)}}{\rho_a^{(n)}} \right)^{\lambda_a} \qquad (3)$$

where λ_a is the heat capacity ratio c_p/c_v .

• The bubble is considered as a perfect gas whose behaviour follows a polytropic law:

$$p_b^{(n+1)} = p_b^{(n)} \left(\frac{\rho_b^{(n+1)}}{\rho_b^{(n)}} \right)^{\eta_b} \qquad (4)$$

The exponent η_b can have any positive value. For instance, $\eta_b = 1$ for an isothermal law or $\eta_b = \lambda_b$ for an adiabatic law.

• Sodium can exist both in a liquid phase and a gaseous phase because of the possibility of cavitation. The diphasic sodium is supposed to be at saturation conditions, and its temperature is assumed to be constant. The liquid is submitted to the pressure:

$$p_s^{(n+1)} = p_g^{(n+1)} = p_s^{(n)} + C_s^2 \left(\rho_s^{(n+1)} - \rho_s^{(n)} \right) \qquad (5)$$

with C_s the sound velocity in sodium. The vapour only depends on the initial temperature $T^{(0)}$:

$$p_v^{(n+1)} = p_{sat} \left(T^{(0)} \right)$$

EUROPLEXUS computes the average density and the concentration of each constituent from the mass conservation for each fraction. Then the pressure of the mixture is obtained by successive iterations. The iterative process computes:

1. The sodium density from (5) by estimating approximately $p_s^{(n+1)}$ at the beginning of the time step,
2. The void fraction and then the argon and bubble densities from (2),
3. The argon pressure from (3),
4. The bubble pressure from (4),
5. The pressure mixture from (1).

4 NUMERICAL MODELING OF THE MOCK-UP

The MARA8 mock-up is composed of structures and fluids interacting with each other. The mock-up includes a flexible vessel with a flexible roof. Structures are assumed to be thin and flexible enough to be represented by shells.

Owing to the symmetry of the mock-up, an axisymmetrical representation was used for the numerical simulation. Figure 3 presents the mesh used for the numerical simulation.

In case of a HCDA, the internal fluids are sodium, argon and a gas bubble. In the test, these fluids are respectively replaced by water, air and an explosive charge. Water and air are initially at atmospheric pressure, whereas the explosive charge induces an initial pressure of 165 MPa in the bubble area.

The characteristics included in the numerical model are:

- Water : $\rho = 998.3$ kg/m3 sound speed $C = 1550$ m/s $p^{(0)} = 10^5$ Pa
- Air : $\rho = 1.206$ kg/m3 $\lambda = c_p/c_v = 1.4$ $p^{(0)} = 10^5$ Pa
- Explosive charge : $\rho = 400$ kg/m3 polytropic coef. $\eta = \lambda = 1.24$ $p^{(0)} = 1.646\,10^8$ Pa

In EUROPLEXUS, fluids and structures can be described with an Eulerian, Lagrangian or A.L.E. approach. In the current numerical simulation, all the structures are represented with a Lagrangian description and the mesh follows the deformation of structures. The grid of water and air is governed by an ALE model: it is updated according to the deformation of the neighbouring structures. The bubble zone is kept fixed. Indeed if the bubble grid were ALE, the mesh would deform very much because of the expansion of the bubble gas at a very high initial pressure and this large deformation would entail numerical difficulties to carry out the computation. Moreover, the fixed bubble grid is used as a reference for the updating of the ALE surrounding mesh.

Two kinds of fluid-structure coupling are available in the EUROPLEXUS code. Their main differences come from the definition of the local normal vector used to write the coupling relations between the freedom degrees of fluid and solid. The first fluid-structure coupling (FS2D instruction) requires the definition of coupling elements by the user, which assigns the same displacements to the fluid nodes and the structure nodes facing each other. The main drawback of this coupling lies in the absence of automatic actualisation of the ALE grid for the elements other than the ones on the coupled lines.

The second coupling (FSA instruction) does not require coupling elements; the code considers directly the fluid and solid nodes in contact and writes relations allowing a possible tangential fluid flow relatively to the structure location. The FSA coupling is well adapted to complex geometries but it often implies a user intervention to pilot the displacements of the fluid ALE grid.

In the CASTEM-PLEXUS simulations performed in the 90s [6], only the FS2D coupling was available. For the previous EUROPLEXUS simulation [35], the FS2D coupling was conserved as the goal was to observe the influence of a thinner mesh. In the current simulation, the FSA coupling was adopted to test the influence of the coupling on the precision of results.

In order to prevent cell crashing in the air zone during the ALE mesh updating, a relation governing the local displacement of the air mesh is defined by the user. This line manages the interface between the water zone and the air layer. The fluid nodes at the interface are forced to remain aligned. Due to the difference of compressibility between air and water, the air zone might suffer a crushing of some cells during the explosion in the absence of this governing line.

Boundary conditions were:
• No horizontal displacement on the symmetry axis,
• No rotation of the two vessel and roof nodes located on the symmetry axis,
• Complete blocking of the node in the top right-hand corner at the junction between the vessel and the roof.

5 RESULTS

The interpretation of the numerical results is based on the analysis of pressure, gas fraction, fluid speed, radial and vertical displacements, stresses and strains versus time. The evolution of these variables is presented on images showing the state of the internal fluids or structures at different times.

5.1 Pressure

Pressure is presented in Fig. 4. Initially, fluid is at atmospheric pressure, apart from the high-pressure gas bubble in the centre of the mock-up. Initial pressure induced by the explosive charge simulating the gas bubble is equal to 165 MPa. The pressurised zone expands spherically, causing the propagation of a pressure wave. During the expansion, the average pressure of the pressurised zone decreases in inverse proportion to the increase in volume. After 0.08 ms, pressure in this zone goes down to 35 MPa.

The first contact of the pressure wave with the mock-up structures occurs at the vessel base after 0.13 ms. As a consequence, the downward expansion of the pressurised area is stopped by the vessel base, and the expansion continues laterally along the vessel base. Owing to the pressure wave rebound against the vessel base, the pressurised zone is pushed back upwards and a low-pressure zone appears above the vessel base. The low-pressure zone appears first next to the symmetry axis (at 0.16 ms) and spreads progressively laterally and upwards. Pressure in this area is approximately equal to atmospheric pressure.

The pressure wave comes into contact with the lateral wall of the vessel after 0.22 ms. At that time, the pressurised area is divided into four zones:
• Near the vessel, a high-pressure zone (about 20 MPa) due to the splashing of the pressure wave against the vessel is observed,
• In the annular strip between 1 / 2 and 3 / 4 of the vessel radius, pressure is lower (7-8 MPa),
• A second pressurised area appears in the periphery of the central zone; this zone is spherical and its pressure is equal to about 14 MPa,
• In the middle of the mock-up, pressure is lower and equal to 7 MPa.

In a first time, pressurisation comes from the the propagation of the acoustic shock wave. This phase ends after approximately at 0.3 ms since the acoustic wave crashes against the lateral wall of the vessel. Because the air layer absorbs the excess pressure at the top of the mock-up, the pressure wave does not bounce back against the roof. Then a second pressurisation phase appears, issued from the acceleration of fluids.

From 0.32 to 0.5 ms, the central hydraulic pressure wave expands and contacts the vessel bottom, inducing a pressure increase up to 12 MPa near the bottom while pressure is equal to only about 3 MPa in the middle.

The pressurised area at the bottom extends progressively along the vessel base towards the lateral wall. When fluid impacts the bottom right-hand corner, it splashes and different hydraulic waves start propagating in different directions. At 0.72 ms, a first reflected wave propagates backwards horizontally along the vessel base. At 0.78 ms, a second reflected wave orients diagonally inwards while a third wave propagates upwards along the lateral wall.

Meanwhile, the central pressurised area expands to some extent and pressure decreases in the middle of this zone. At 0.84 ms, the centre of the mock-up is depressurised (1 MPa) and surrounded by a 2.5 MPa sphere. The diagonally reflected wave joins the central wave and the bottom reflected wave arrives at the symmetry axis.

Between 0.9 and 1.2 ms, due to the projection of fluid from the centre of the mock-up towards the vessel base and the lateral wall, the fluid already present in this area cannot flow inwards and thus pressure increases. The pressurised area extends from mid-radius to the lateral wall and the vessel base. The average pressure is equal to 3 MPa but, at one location, pressure reaches 16 MPa.

As fluid orients progressively upwards near the lateral wall and as fluid also impacts the roof near the symmetry axis, the pressurised area spreads upwards along the lateral wall and below the roof. At 2.4 ms, the pressurised area has a spherical shape with a depressurised centre. Pressure is distributed along the vessel base and the lateral wall and from the symmetry axis to mid-radius below the roof.

Between 2.4 and 3.3 ms, as fluid orients preferentially upwards and a bit downwards, pressure concentrates in the upper and lower parts of the mock-up. Half-way up, the mock-up is depressurised. At 3.3 ms, pressure is localised in the bottom left-hand corner limited by the vessel bottom and the symmetry axis and in the top right-hand corner limited by the roof and the lateral wall. At that time, fluid is expelled from the centre towards the top and bottom parts of the mock-up. As fluid cannot flow from both corners, pressure increase in these areas.

From 4 to 5 ms, the fluid flows are illustrated by the evolution of the pressure map: fluid is expelled from the top right-hand corner towards the top left-hand corner. Consequently, a displacement of the pressurised area below the roof is observed towards the symmetry axis and a pressure peak up to 18 MPa in the top left-hand corner at 4.4 ms.

Afterwards, pressure is very low in the mock-up and it is more difficult to follow the pressure evolution.

5.2 Gas fraction

Figure 5 presents the volumic presence fraction of gas. In order to interpret correctly the presence of each constituent, the massic presence fractions of the bubble and air are described in Figs. 6 and 7.

Initially, the gas is located in the middle of the mock-up (the bubble) and below the roof (air). The gas bubble expands spherically until 0.8 ms. During the passing of the acoustic wave (until 0.3 ms), water remains liquid. Due to the depressurisation following the acoustic wave passing, water vaporises slightly and steam trails are observed in the depressurised areas:

- Above the vessel base at about 0.3 ms,
- Roughly between mid-radius and the lateral wall and below the air layer.

The air layer remains unchanged as long as the shock wave does not reach the upper part of the mock-up. From 0.2 ms, the bottom of the air layer begins to be compressed upwards near the symmetry axis.

From 0.8 to 2 ms, the bubble goes on expanding but no longer uniformly. As the bubble gas flows preferentially along the vertical axis and horizontally, the presence fraction of the bubble is lower along these three directions than in the other directions. Steam condenses and the gas bubble becomes surrounded only by liquid water. Progressively, the air layer is compressed upwards and pushed towards the top right-hand corner.

From 2 to 4.5 ms, the bubble gas goes on expanding but mainly shifts upwards as water rebounds on the vessel base and pushes the bubble upwards. Water is fully liquid everywhere. At about 4 ms, the air is completely flattened in the top right-hand corner and the size of the air bag has become minimal.

Between 4.5 and 8 ms, as the upward progression of the bubble is limited by the roof, the bubble spreads preferentially sideways. Due to the expansion of the bubble, the local gas ratio decreases. There is a gaseous layer above the vessel base which may be composed of steam. The air bag in the top right-hand corner is pushed back by the external structures of the mock-up and the air expands along the roof. At 8 ms, two air bags are observed: one remaining in the top right-hand corner and a second one near the symmetry axis.

From 8 to 14 ms, the central bubble gas divides into two parts with a diagonal cut. The separation corresponds to violent water flows oriented towards the centre of the mock-up. The concentration of the bubble gas is higher in the upper bag than in the lower bag. Little by little, the lower bag disappears whereas the upper bag spreads downwards. At 14 ms, the bubble bag has a "S" shape.

The steam layer along the vessel base persists. The air bag near the symmetry axis blurs progressively. The air bag in the top right-hand corner expands downwards along the lateral wall.

Until 20 ms, the bubble gas goes on extending downwards with the same "S" shape. The central part of the "S" becomes thiner while gas concentrates in the "S" extremities. Due to the compression exerted by the downward arrival of the pressurised bubble, the steam layer at the bottom condenses. The air layer expands more and more horizontally along the roof and vertically along the lateral wall.

5.3 Fluid velocity

Figure 8 shows the local flow orientation in the mock-up. Figure 9 indicates the intensity of velocity. Initially, all the fluids are at rest. From 0.02 ms, the explosion violently expels the bubble gas and water in the vicinity from the central area. The fluid velocity is very high: up to 260 m/s. Until 0.12 ms, fluid moves with a uniformly spherical velocity. At that time, the vessel base is impacted by fluid.

From 0.12 to 0.4 ms, the explosive gas and water continue to expand radially and upwards at a rate going from 150 m/s in the centre of the mock-up to 40 m/s near the vessel base. The full vessel base is impacted after 0.2 ms, the lateral wall and the roof after 0.4 ms. The norm of the velocity is no longer uniform. The velocity is very high (up to 200 m/s) on the symmetry axis in the bubble area. The velocity is higher in the centre, at the bottom near the vessel base and just below the air layer than near the lateral wall and in the air layer. In the air zone, velocities are oriented upwards and remain limited to 10-30 m/s.

From 0.5 to 1.5 ms, the bubble gas and water go on expanding spherically in the centre. Near the lateral wall, fluid starts deviating and flows slowly upwards. The fluid trapped in the bottom right-hand corner starts flowing along the vessel base towards the central axis. At the top of the mock-up, the air is pushed horizontally towards the top right-hand corner joining the vessel and the roof. Velocities are higher:

- In the centre upwards and downwards along the vertical axis (180 m/s),
- On a sphere whose radius is equal to 1/3 of the vessel radius (80 m/s),
- In a horizontal channel at mid-height joining the centre to the sphere.

Between 1.5 and 3 ms, several fluid orientation changes occur. The fluid in the centre starts moving upwards. The fluid in the lower part of the mock-up flows towards the symmetry axis and concentrates in the bottom left-hand corner. Speeds are much higher in the upper part of the mock-up (up to 60 m/s) than in the lower part (less than 20 m/s). Water flows upwards along the lateral wall and in the upper part of the mock-up near the symmetry axis. The air and water below the roof are propelled towards the top right-hand corner with speeds up to 200 m/s in the corner.

Between 3.5 and 4.5 ms, fluid orients massively from the bottom towards the top of the mock-up. Some kind of sharing line appears at mid-radius: the fluid in the centre flows towards the symmetry axis and then upwards with a rotating motion while the fluid in the periphery flows slightly outwards and mainly upwards. High speeds (up to 140 m/s) are recorded in the middle of the mock-up. Near the top of the lateral wall, water flows outwards and impacts the wall horizontally what will induce the formation of a upper bulge. The sharing line continues in the upper part of the mock-up: while the water located near the vessel flows towards the vessel, the water at mid-radius goes back towards the symmetry axis. Globally, the velocities near the vessel are much lower than in the centre. The air is still hurled horizontally along the roof towards the top right-hand corner.

From 5 to 10 ms, between the axis and mid-radius, water globally flows towards the mock-up centre, thus inducing the beginning of a twirling flow with speeds reaching 80 m/s. Near the lateral wall, water rebounds on the roof and goes down along the wall. Below the roof, there are two contradictory flows: along the roof, air flows outwards whereas just below water and air flow inwards.

Between 11 and 15 ms, flows change direction very locally in the centre. The fluid coming from the top flows towards the centre. Just above the middle of the mock-up, the bubble goes upwards near the axis and downwards with a rotating motion at a quarter of the radius. Just below mid-height, the fluid at a quarter of the radius is ejected with an out-down orientation. The fluid pushed by the previously cited flow is expelled with an in-down orientation towards the bottom left-hand corner. Both flows reproduce a "S" shape. Along the lateral wall, fluid flows down and continues inwards along the vessel

base. Below the roof, the sharing line is located at one third of the radius, so that air and water flows towards both top corners. The highest velocities are located in the bottom left part of the mock-up and are lower than 35 m/s.

From 16 to 20 ms, the central flows orient more and more upwards near the axis while fluid whirls round at mid-radius. In the lower part, fluid completely changes direction and now flows downwards, goes outwards along the vessel base and finally goes up along the lateral wall. Below the roof, the air orients outwards; the concentration in the top right-hand corner induces the formation of an air whirlpool. Velocities are lower than 30 m/s in the whole mock-up.

5.4 The deformed shape

The deformed shape of the mesh is presented in Fig. 10. The first deformation occurs in the bubble area quite immediately and then in the vicinity of the bubble area. After 0.5 ms, the cells below the bubble and the vessel base lower due to the pressure wave impact and the fluid acceleration. The vessel base deformation increases throughout the computation and represents the most important structure displacement. The bottom right-hand corner of the vessel becomes more rounded and opens as it is pulled down by the vessel base. Laterally, cells at mid-radius present a kind of bending and corners become more rounded. Below the air layer, the cells are compressed upwards near the symmetry axis.

Between 0.5 and 2 ms, we note the same global deformation of inner cells. The vessel base lowers first near the symmetry axis and then it flattens from the axis to mid-radius as the location of the impact of fluid shifts along the vessel. The bottom right-hand corner becomes completely rounded. The lateral wall starts deforming radially: a large bulge appears approximately half-way up the height of the mock-up because of the impact, perpendicularly to the vessel, of fluid expelled from the mock-up centre. The roof starts going up near the symmetry axis.

From 2 to 3.5 ms, as the fluid thrust on the vessel base concentrates towards the symmetry axis, the vessel base points down near the axis. The upward flows along the lateral wall induce an extension of the area concerned by the lower bulge. As fluid flows concentrate in the top right-hand corner, a second bulge (called upper bulge) appears at 3.5 ms in the upper part of the vessel near the junction with the roof. Progressively, the entire roof is lifted, due to the upward thrust of the fluid coming from the central part of the mock-up. The deformation is maximal on the symmetry axis and decreases towards the roof edge.

From 4 to 6 ms, the mesh deformation concentrates in the upper part of the mock-up. The upper bulge shifts and extends a little downwards: as fluid is still flowing up along the lateral wall and as its evacuation along the roof is very limited, the vessel wall bends. The deformation is concentrated in a small area but its amplitude is more important than the one of the lower bulge. Due to the upward flow, the ALE updating of mesh leads to a compression of some cells in the initial air layer below the roof.

From 8 to 20 ms, the cell shape becomes more regular in the upper part of the mock-up. Globally the mesh does not evolve much.

5.5 Radial displacements of structures

Figure 11 shows the radial displacements of structures. The first displacement appears at the bottom of the lateral wall, just above the bottom right-hand corner: it is equal to about 5 mm after 0.5 ms. Then the deformed zone extends upwards and the maximum displacement shifts at one third of the height of the lateral wall from the bottom right-hand corner. The maximal displacement reaches approximately 16 mm after 2 ms. This radial displacement corresponds to the formation of the lower bulge in the lateral wall.

A second radial displacement appears in the vessel base at mid-radius from 1.5 ms. The size of the deformed zone and the value of the displacement increase until 3 ms. At that time, the displacement reaches a maximal value of 7 mm. Then the radial displacement remains constant. This displacement comes from the downward deformation of the vessel base.

A third radial displacement occurs in the upper part of the lateral wall from 3.5 ms. The extension of the deformed area and the amplitude of the displacement increase until 5 ms. At that time, the maximal value reaches 20 mm. Then this displacement remains constant until the end of the simulation. This displacement is due to the creation of the upper bulge in the lateral wall.

No radial displacement is observed in the roof because of the modeling, the node in the top right-hand corner being completely blocked.

5.6 Vertical displacements of structures

Vertical displacements are shown in Fig. 12. A downwards displacement is observed in the vessel base during the whole simulation. It starts near the symmetry axis and extends progressively to the whole vessel base. The maximal amplitude, equal to 55 mm, is reached at 3 ms and remains constant until the end of the computation. This displacement corresponds to the downwards deformation of the vessel base.

From 2.5 ms, an upwards displacement occurs in the roof. It starts on the symmetry axis and extends towards the roof edge. The maximal value is observed on the symmetry axis and is equal to about 30 mm from 6 ms. The distribution of displacements in the roof evolves slightly afterwards: displacement goes on increasing until 10 ms before decreasing a little. This upwards displacement is due to the roof lift under the upward fluid thrust.

Between 1.5 and 3.5 ms, the lower part of the lateral wall moves down. The wall is pulled down by the downward bending of the vessel base. The size of the subsided area extents until 3 ms to reach half-way up, then the deformed size reduces and finally disappears. This lowering remains limited to 5 mm.

At 4 ms, the lateral wall takes again its initial location: it is in equilibrium between the downward thrust exerted on the vessel base and the upward thrust applied to the top right-hand corner. From 4.5 ms, the upper part of the lateral wall and then the full lateral wall are pulled upwards, probably as a consequence of the upwards fluid flows along the wall and of the upper bulge formation. This displacement cannot be caused by the roof lift owing to the complete blocking of the point in the top right-hand corner. The displacement amplitude remains limited to 5 mm.

5.7 Von Mises stresses in structures

Figure 13 illustrates the evolution of stresses versus time. Stresses appear first in the vessel base, near the symmetry axis, when the pressure wave hits the vessel base and then propagates along the vessel. Stresses reach very quickly 500 MPa near the symmetry axis and remain constant at that location until 0.3 ms.

The whole vessel base and the whole lateral wall become submitted to stresses from 0.2 ms and 0.28 ms, respectively. The stress increase coincides with the arrival of the acoustic pressure wave. From 0.24 ms, three high stress spots appear near the bottom right-hand corner. These spots correspond to the junctions between the two vessel parts of reduced thickness and the rest of the vessel.

Between 0.3 ms and 0.4 ms, if stresses decrease slightly in the vessel base, they increase in the lateral wall and concentrate in the bottom right-hand corner. During this phase, the passing of the acoustic pressure is ended and the expansion of the hydraulic wave is still limited to the centre of the mock-up.

From 0.4 to 1.5 ms, stresses increase in the whole vessel due to the massive splashing of fluid against the lateral wall and the vessel base. The average value of stresses is around 500 MPa in the vessel base and 300 MPa in the lateral wall. From 0.8 ms, two spots of higher intensity appears in the upper part of the lateral wall; they coincide with a curve change of the shell induced by the formation of the lower bulge. In the bottom corner, stresses are much higher as the corner is opening due to the downward tension exerted by the vessel base lowering. Stresses reach 700 MPa in the corner, with local spots of 1100 MPa and 1300 MPa at the top and bottom junctions of thickness changes surrounding the corner.

Between 1.6 and 2.4 ms, as the maximum impact of flows against the vessel base shifts from mid-radius towards the symmetry axis, stresses decrease in the vessel base between mid-radius and the bottom corner. Stresses remain constant in the bottom right-hand corner and in the upper part of the lateral wall. At the bottom of the lateral wall, the stress level decreases slightly as fluid flows changes direction: they stop impacting the wall perpendicularly and orient rather upwards. Due to the impact of the roof by upwards flows, stresses appear first near the symmetry axis at 1.6 ms and extend progressively to the entire roof.

Until 3.2 ms, stresses go on decreasing in the vessel base. However, due to the final concentration of fluid near the symmetry axis, stresses present a temporarily local rise at 3 ms near the axis. In the bottom right-hand corner, stresses start decreasing after 3.2 ms. The three high stress spots in the vessel base disappear. Whereas stresses decrease in the lower part of the lateral wall, they increase in the upper part. Indeed, fluid along the lateral wall flows upwards and concentrate near the top right-hand corner. The formation of the upper bulge is preceded by a stress increase and the formation of three high stress spots. The junction between the vessel and the roof becomes a plastic kneecap. Stresses in the roof increase and their distribution becomes more regular: about 300 MPa at 3.2 ms.

Between 3.2 and 5 ms, stresses reduce progressively in the vessel base and the lower part of the lateral wall. In the upper part of the mock-up, stresses increase until 4 ms and then start decreasing. The stress level reaches a highest value of 900 MPa at 4 ms in the three spots located in the upper part of the lateral wall. Apart in the top right-hand corner where fluid still impacts the lateral wall, fluid globally flows towards the centre of the mock-up after it has rebounded on the external structures. This is the reason why stresses globally decrease in the vessel and the roof.

Between 6 and 10 ms, stresses decrease considerably as flows are globally oriented inwards. Stresses remain lower than 200 MPa in the roof and in the vessel base and 150 MPa in the lower part of the lateral wall. Structures present two hinges with higher stresses. In the top right-hand corner, stresses decrease progressively from 400 down to 300 MPa. In the bottom right-hand corner, stresses remain constant and equal to 400 MPa.

Between 11 and 14 ms, stresses remain relatively constant in the roof: 150 MPa from the axis to mid-radius and 200 MPa from mid-radius to the top right-hand corner. Stresses increase in the upper part of the lateral wall to reach locally 700 MPa at 14 ms. Stresses are a higher near the top right-hand corner because flows under the roof are separated by a sharing line: the flows in the left part are oriented towards the symmetry axis and then deviate downwards whereas the flows in the right part are oriented outwards and remain trapped in the corner.

In the lower part of the lateral wall, stresses remain lower than 150 MPa. In the vessel base, stresses remain lower than 200 MPa, except at two points. Stresses at the point located at 1/3 of radius reach 200 MPa while stresses at the point located at 2/3 of radius reach 450 MPa. These two high-stress points are the consequence of the central whirlpool in 'S' which impacts the vessel base approximately at mid-radius.

Between 14 and 16 ms, we note a global stress increase which reaches a maximum at 15 ms, followed by a stress decrease. Stresses reach 900 MPa at the two spots in the upper part of the lateral wall. This stress peak is the consequence of the continuous accumulation of fluid in the top right-hand corner from 8 to 15 ms. As fluid compressed in the corner succeeds in flowing down along the wall from 16 ms, stresses start decreasing from that time.

Simultaneously, the vessel base and the bottom right-hand corner are submitted to a high increase of stresses as the central 'S' flows propel violently fluid against the vessel base. Stresses reach 700 MPa at 15 ms in the bottom right-hand corner and 500 MPa not far from the symmetry axis. As the central flow leads to the formation of a whirlpool twirling around its own axis from 16 ms, the vessel base becomes less in demand from that time and stresses decrease in the vessel base from 16 ms.

From 17 ms, stresses become much lower in all structures. They are globally included in 150 to 200 MPa, except in the bottom right-hand corner where a high stress point persists at 250-300 MPa.

5.8 Plastic strains in structures

Figure 14 presents the plastic strains. The first plastic strains happen after 0.4 ms in the vessel base near the symmetry axis, at the bottom of the lateral wall, in the bottom right-hand corner and in the top right-hand corner. These strains correspond respectively to the lowering of the vessel base, to the formation of the lower bulge in the lateral wall, to the opening of the bottom right-hand corner and to the impact of fluid in the top right-hand corner.

From 0.8 to 1.6 ms, plastic strains increase in the vessel, particularly:
• in the half part of the vessel base comprised between the symmetry axis and mid-radius as this part is close to the bubble area and directly submitted to the impact of fluid expelled from the central area,
• in the bottom right-hand corner where one point acts as a kneecap and allows the opening of the corner: plastic strains concentrate at that point and the part of the vessel base comprised between mid-radius and the bottom right-hand corner seems to be protected,
• in the lower part of the lateral wall, what coincides with the formation of the vessel base.

Between 1.6 and 2.5 ms, plastic strains increase slightly in the lateral wall to reach 6 % at the level of the lower bulge. The strain increase in the vessel base and the bottom corner is much higher. A maximal plastic strain of 8 % is reached in the bottom right-hand corner after 2.5 ms and persists until the end of the simulation: this strain corresponds to the opening of the bottom right-hand corner and is reached very locally. In the rest of the bottom corner, the plasticity level remains lower than 3 % and part of the vessel vase never suffers plasticity. As the downward fluid impact on the vessel base is concentrated on a small area located approximately at one third of radius between 2 and 2.5 ms, there is a neat increase of the plastic strains up to 10 % in that area of the vessel base.

Between 2.5 and 3.5 ms, plastic strains increase in the vessel base near the symmetry axis as the maximal impact of fluid shifted towards the axis. Maximal plastic strains, equal to 16 % in the vessel base on the symmetry axis, are reached after 3 ms. Due to the compression of fluid in the top right-hand corner, the upper part of the lateral wall suffers increasing plastic strains which will lead to the formation of the upper bulge.

From 4 to 6 ms, plasticity increases mainly in the upper part of the lateral wall. The point located in the top right-hand corner becomes a plastic kneecap whose plasticity level reaches 9 %. In parallel, two points located on both sides of the upper bulge suffer high plastic strains. Their maximal value is equal to 16 % and coincides with the location of the maximal radial displacement of the lateral wall. The roof starts suffering plastic strains from 4 ms near the symmetry axis and from 3.5 ms in the close vicinity of the top right-hand corner. From 4 to 6 ms, plastic strains progress in the roof from the axis towards the edge. Plastic strains in the roof remain maximal on the symmetry axis where they reach 2 %.

Between 6 and 20 ms, there is no evolution of the plastic strains in the structures surrounding the mock-up. Fluid impacts on the external structures after 6 ms are not violent enough to induce additional plastic strains.

6 COMPARISON WITH THE EXPERIMENTAL RESULTS AND WITH PREVIOUS NUMERICAL RESULTS

The purpose of our computations consists in validating the HCDA constitutive law of the EUROPLEXUS code and in estimating the progress realised in the modeling of the accident. Thus the current numerical results are compared with the experimental results and the previous numerical results computed with the codes SIRIUS [12], CASTEM-PLEXUS [6] and EUROPLEXUS [?].

The comparison concerns:
• The vertical displacement of the vessel base and the instant of the maximal displacement,
• The hoop strain of the vessel upper bulge, the instant of the maximal strain and the distance to the roof,
• The hoop strain of the vessel lower bulge and the instant of the maximal strain,
• The vertical displacement of the roof and the instant of the maximal displacement,
• The impact pressure on the roof and the instant of the maximal pressure.

Figures 15 and 16 present the vertical displacements of the vessel base (on the symmetry axis) and the roof (in the centre and at mid-radius) for the EUROPLEXUS computations. Figures 17 and 18 show the maximal radial displacements for the upper bulge and the lower bulge for the EUROPLEXUS computations. Previous EUROPLEXUS results between 0 and 7 ms are indicated with bold lines and current EUROPLEXUS results between 0 and 20 ms are drawn with narrow lines.

Figures 19 and 20 display pressure for the MARA8 experiment and for the CASTEM-PLEXUS calculations, respectively. The pressure computed by EUROPLEXUS is presented in Figs. 21 to 25. Previous EUROPLEXUS results are drawn with bold lines and current results with narrow lines. Results are collected in Table 1. The CASTEM-PLEXUS computations, the old EUROPLEXUS ones and the new EUROPLEXUS ones are noted CP, EP1 and EP2 in this table.

The SIRIUS results used for the comparison correspond to computations based on dynamic strain-stress curves [12]. The main difference between the old EUROPLEXUS and CASTEM-PLEXUS computations comes from the mesh fineness. The new EUROPLEXUS simulation benefits from improvements in the treatment of the fluid-structure coupling. Figure 26 illustrates the mesh used in the CASTEM-PLEXUS simulation. The mesh used for both EUROPLEXUS computations is shown in Fig. 3. Figures 27 and 28 present the deformed shape of the mesh at the end of the previous and current EUROPLEXUS simulations. Figures 29 to 32 show a comparison of the flow orientations at 3ms and 7 ms for both old and new EUROPLEXUS simulations.

By comparing figures presenting the displacements computed with EUROPLEXUS, it appears that the vertical displacements are a bit higher on the symmetry axis with the new simulation. On the contrary, the radial displacements are lower for the lower bulge and identical for the upper bulge. By comparing the shape of the deformed meshes, it seems that the new fluid-structure coupling softens structures: deformations are more marked and evolve more locally.

Concerning the vessel base, the vertical displacements on the symmetry axis are higher with the current simulation than the ones issued from the previous EUROPLEXUS computation. The current results are less precise than the ones computed with all the previous simulations. The new EUROPLEXUS results present a 27 % error for the maximal vertical displacement and a 15 % error for the final displacement. The previous EUROPLEXUS simulation was much precise: 15 % and 3.8 the SIRIUS ones (2 % error). Regarding the instant of the maximal displacement, the precision increases slightly from the CASTEM-PLEXUS simulation to the new EUROPLEXUS one, but the SIRIUS simulation was the best one.

Regarding the hoop strain of the upper bulge, the new simulation superimposes exactly with the one issued from the previous EUROPLEXUS simulation. Consequently, the maximal hoop strain is identical (24 % error). Due to the longer duration of the new simulation, the final strain is a bit more accurate than the one computed previously with EUROPLEXUS. These results are less precise than the CASTEM-PLEXUS ones (11 % error) whereas the CASTEM-PLEXUS simulation used a rougher mesh and a simpler fluid-structure coupling. But globally the EUROPLEXUS and CASTEM-PLEXUS results are more precise than the SIRIUS ones (30 % error).

The instant corresponding to the larger upper bulge is a bit late for the EUROPLEXUS and CASTEM-PLEXUS calculations (between 5.3 and 5.6 ms instead of 5.0 ms in the test) while the time computed by SIRIUS is correct (5.1 ms). Concerning the distance between the upper bulge and the roof (4.8 cm in the experimental device), we can note a neat improvement from the CASTEM-PLEXUS simulation (7.3 cm) to the new EUROPLEXUS simulation (6.0 cm). However, these results are not so good as the ones indicated by SIRIUS as this code found almost the right value (5.0 cm).

Concerning the strain of the lower bulge, the three CASTEM-PLEXUS and EUROPLEXUS simulations indicate results in the same order of magnitude and similar to the experimental results (6 % error for the maximal strain and 4.7 % error for the final strain). These results are much better than the SIRIUS ones (18 % error). The instant corresponding to the maximal strain is identical for the three PLEXUS simulations. It is less precise than the ones assessed by SIRIUS which fits exactly with the test.

The roof displacement calculated on the symmetry axis increases from the CASTEM-PLEXUS to the current EUROPLEXUS simulation. As a consequence, the maximal displacement is closer to the experimental value (7.8 % error) but the final displacement is less precise (10.7 % error). Regarding the displacement at mid-radius, the current EUROPLEXUS results fit quite well with the MARA 8 test, as well for the maximal displacement as for the final one. The SIRIUS results were the best ones regarding the roof displacements; nevertheless, the last EUROPLEXUS estimations are very close to the SIRIUS ones. Concerning the time of the maximal displacement, the three codes provide results very close to the experimental result. Globally, the prediction of the roof behaviour was improved by the new simulation.

Concerning the pressure under the roof, the CASTEM-PLEXUS and EUROPLEXUS simulations were able to represent the two experimental peaks. The instant of the maximal pressure for each peak fits perfectly with the experimental results, but the peak amplitude is not correct. The computed first peak is much lower and much larger than the experimental one (5.2 MPa in the centre, 5.5 MPa at one quarter of the radius, 4.2 MPa between mid-radius and the roof edge in the new EUROPLEXUS simulation, instead of 18 MPa in the test). Nevertheless, we can remark that the amplitude of the first peak increases from the CASTEM-PLEXUS to the last EUROPLEXUS simulation. Even if the numerical prediction remains much lower than the experimental value, it appears that the mesh and fluid-structure coupling improvements lead to an improvement of the pressure results.

For the second peak, the computation shows a high and thin peak in the centre (22 MPa) and larger peaks elsewhere (6.2 MPa) whereas the test presents a succession of small peaks. Apart from the centre, the top value of the simulated second peak presents a good similarity with the experimental values.

One can remark that, on the symmetry axis, the second peak has a very different shape from anywhere else under the roof. The amplitude of the computed second peak in the roof centre is a consequence of the high vertical speeds observed for the fluid on the symmetry axis.

To summarise, the new simulation improved the prediction of the roof displacement, the final displacement of the upper bulge, the pressure under the roof and the distance to the roof of the upper bulge. Estimations concerning the lower bulge and the instants of maximums globally did not change. The prediction of the vessel base displacement worsens.

By comparing the EUROPLEXUS estimation with the test, it appears that the displacements computed for the roof and of the lower bulge are in good agreement with the experiment whereas the ones predicted for the upper bulge and the vessel base are not good.

Regarding the pressure at the centre of the roof, the maximal values computed seem to be reversed between both peaks. In the MARA 8 test, the high pressure peak corresponds to the impact of the acoustic wave whereas, in the EUROPLEXUS simulation, it corresponds to the impact of fluid splashing on the roof. If one compares the second peaks observed in the experiment and in the simulation anywhere else than on the symmetry axis, the results are in a good agreement.

It is not easy to conclude about the agreement or not of the simulated pressures with the test because Cariou indicated in ref. [6] that the pressure measurement in the mock-up lacked precision. That could partially explain the differences between the computed and experimental results. Moreover, as the pressure computed with SIRIUS is not available in [12], it is difficult to assess the precision of the simulation without reliable reference data.

The comparison with the SIRIUS results shows that, in some cases, the EUROPLEXUS results are better than the SIRIUS ones and, in other cases, the SIRIUS results fit better with the experimental ones.

Globally, the results issued from the EUROPLEXUS simulation are a bit better than the CASTEM-PLEXUS ones. Some discrepancies persist and there is no obvious method to improve them. But the gaps observed are relatively limited. Therefore, we can conclude that the four sets of numerical results are in good agreement with the test.

7 DISCUSSION

In this part, a synthesis of the results computed with the current EUROPLEXUS model is presented.

Initially, air and water are at atmospheric pressure whereas pressure in the central bubble is equal to 166 MPa. All fluids are at rest. The gas bubble starts expanding immediately and an acoustic pressure wave propagates spherically.

The water in the periphery of the bubble is accelerated with speeds up to 200 m/s at 0.02 ms at the interface water-bubble. The pressure wave impacts the vessel base at 0.14 ms, causing a lowering of the vessel base. Stresses increase in the base but the behaviour of the base remains elastic.

From 0.14 ms to 0.28 ms, the pressure wave moves laterally. It crashes against the lateral wall from 0.2 ms. The main impact occurs in the lower part of the wall, what induces a radial bending of the wall from the bottom right-hand corner to mid-height. Stresses increase particularly in the bottom right-hand corner.

Between 0.3 ms and 1.5 ms, a hydraulic pressure wave propagates through the mock-up. It corresponds to the expansion of the gas bubble. Until 0.5 ms, the bubble expands spherically and fluid impacts the entire external structures. Water vaporises slightly due to a temporary pressure decrease near the lateral wall.

At 0.5 ms, the hydraulic wave impacts the vessel base for the second time. Stresses increase again near the symmetry axis and strains in the vessel base start becoming plastic. Between 0.5 and 0.75 ms, the pressure wave moves radially along the vessel base towards the bottom right-hand corner. The air layer starts being compressed upwards against the roof by the water propelled outwards by the bubble expansion. Stresses increase especially in the bottom right-hand corner and plastic strains appear in the corner and in the lower part of the lateral wall.

Between 0.8 and 1.5 ms, the pressure wave goes up along the lateral wall. Due to the expansion of the gas bubble, the centre of the bubble becomes depressurised and the bubble density increases in the periphery of the initial bubble location. Besides, steam condenses near the lateral wall and the violent compression of the air layer near the symmetry axis induces a horizontal expulsion of air along the roof towards the lateral wall.

Concerning structure deformations, the vessel base continues to lower, particularly at one third of the radius. The lateral wall bends radially, which causes the formation of a lower bulge. The roof starts rising near the symmetry axis. The entire vessel undergoes plastic strains while the roof is still spared.

Between 1.5 and 3.5 ms, the bubble expands vertically, especially upwards. After water rebounded on the bottom right-hand corner, it shares into three flows:
• One goes back along the vessel base and pushes water towards the symmetry axis, causing a local lowering of the vessel base versus the location of the maximal impact,
• Another goes up along the lateral wall, what increases the lower bulge deformation (the maximal radial displacement of the lower bulge is reached at about 2 ms),
• The last one rebounds towards the centre of the mock-up and pushes upwards all the fluid in the centre; as a consequence, the roof undergoes a first pressure peak and bends upwards, and the air bag is strongly compressed in the top right-hand corner.

Between 3 and 5 ms, the bubble goes on extending upwards and the gas concentrates in the top of the panache. The fluid flows massively upwards with a sort of sharing line at mid-radius. The fluid on the right side flows upwards and partly outwards, whereas the fluid on the left side converges towards the centre, which contributes to push up the gas bubble.

Along the roof, fluid is deviated from the axis towards the roof edge. The convergence, towards the top right-hand corner, of the horizontal flows below the roof and of the upwards flows along the lateral wall leads to a high and localised bending of the upper part of the lateral wall. The roof undergoes a second pressure peak around 4 ms. The maximal vertical displacements of the vessel base and the roof are recorded at 3.2 ms and 4.6 ms, respectively.

From 5 to 8 ms, the central gaseous area diffuses in the vicinity and the gas bubble spreads horizontally and then slightly downwards and outwards. The fluid located in the vicinity of the external structures is propelled towards the centre and concentrates in the middle of the mock-up. Therefore, two flows form in the middle: an upwards flow near the symmetry axis and a downwards-outwards flow a bit farther.

Due to the depressurisation occuring next to structures, the air bad starts expanding and goes back inwards along the roof and moves slightly down along the wall. The upper bulge becomes a bit more marked radially and extends a bit downwards. The maximal radial displacement is reached at 5.5 ms for the upper bulge. Simultaneously, the roof is lifted.

Between 8 and 14 ms, the central upwards flow continues along the symmetry axis while the downwards-outwards one at mid-radius takes an undulate shape (a sort of "S") under the effect of two contradictory forces. The fluid flowing up along the axis shifts the flow at mid-radius, whereas the fluid coming from the roof or the lateral wall pulls inwards the flow at mid-radius.

In the centre of the mock-up, the gas bubble splits up into two bags under the influence of both central flows in opposite directions. Little by little, the lower bag disintegrates and the upper bag takes an "S" shape. The air bag in the top right-hand corner inflates because the air below the roof flows back towards the corner and because of the depressurisation near structures. Globally, the external structures do not deform more: the final deformed shape of the mock-up is reached at 10 ms.

After 15 ms, the bubble expands, stretches upwards and downwards but keeps its "S" shape. A whirlpool forms at the base of the "S". Air below the roof flows towards the top right-hand corner and then deviates downwards along the lateral wall. The air bag extends.

At 20 ms, the resistance of water leads to the formation of a whirlpool in the air zone, just below the top right-hand corner. Stresses decrease in structures and become lower than 250 MPa after 20 ms.

8 CONCLUSION

In this paper, a computation of the MARA8 test simulating a Hypothetical Core Disruptive Accident is presented. The test consists in an explosion inside a steel vessel with a flexible roof. An explosive charge is placed in the middle of the mock-up. The vessel is filled with water, topped by an air layer below the roof. A specific HCDA constitutive law has been developed in the EUROPLEXUS code to simulate this kind of explosion.

The code computed successfully the explosion during 20 ms of physical time. The simulation shows the propagation of a pressure wave from the explosive zone towards the external vessel. A large gaseous zone appears in the middle of the mock-up. The pressure wave impacts first the vessel base and then the lateral wall. A large lower bulge forms in the lower part of the vessel lateral wall.

Then water is pushed back by the vessel, goes upwards and impacts the roof. The roof undergoes two high-pressure peaks and is lifted. The air layer is expelled in the top right-hand corner by the upwards flows of water. A second bulge appears in the upper part of lateral wall.

A comparison is realised between the experimental results and numerical results provided by several computations: two simulations with the EUROPLEXUS code, one with the CASTEM-PLEXUS code, and one with the SIRIUS code. Globally the results of the four simulations are in good agreement with the experimental results.

The new EUROPLEXUS simulation improves the accuracy of assessments in some parts of the structures. But some discrepancies persist in other parts and there is no obvious solution to get a better precision.

Generally speaking, the new fluid-structure coupling tested in the current simulation improves much the global mesh deformation and changes considerably the flow orientations in the mock-up after the rebound of the fluid against the structures.

References

[1] D. Acker, A. Benuzzi, A. Yerkess, J. Louvet. MARA 01/02 - Experimental validation of the SEURBNUK and SIRIUS containment codes. In: *6th Int. Conf. on Structural Mechanics In Reactor Technology*, Section E3/6. Paris, France, 1981.

[2] C. Albertini, et al. The JRC-COVA programme : Final Report. Commission of the European Communities, Report EUR 8705. *Nuclear Science and Technology*: 1-182, 1984.

[3] A. Benuzzi. Comparison of different LMFBR primary containment codes applied to a benchmark problem. *Nuclear Engineering and Design*, **100**: 239-249, 1987.

[4] Y. Blanchet, P. Obry, J., Louvet. Treatment of fluid-structure interaction with the SIRIUS computer code. In: *Proc. 6th Int. Conf. on Structural Mechanics In Reactor Technology*, Section B8/8. Paris, France, 1981.

[5] C. Bour, M. Spérandio, J. Louvet, C. Rieg. LMFBR's core disruptive accident. Mechanical study of the reactor block. In: *Proc. 10th Int. Conf. on Structural Mechanics In Reactor Technology*, Vol. E, 281-287. Anaheim, USA, 1989.

[6] Y. Cariou, M. Spérandio, M. Lepareux, K. Christodoulou. LMFBR's whole core accident. Validation of the PLEXUS code by comparison with MARA tests. In: *Proc. 12th Int. Conf. on Strructural Mechanics In Reactor Technology*, Section E7/4. Stuttgart, Germany, 1993.

[7] Y. Cariou, J.P. Pirus, C. Avallet. LMR large accident analysis method. In: *Proc. 14th Int. Conf. on Structural Mechanics In Reactor Technology*, Section P3/7, 395-402. Lyon, France, 1997.

[8] F. Casadei, A. Daneri, G. Toselli. Use of PLEXUS as a LMFBR primary containment code for the CONT benchmark problem. In: *Proc. 10th Int. Conf. on Structural Mechanics In Reactor Technology*, Section E13/1, 299-304. Anaheim, USA, 1989.

[9] C. Chavant, A. Hoffmann, P. Verpeaux, J. Dubois. Plexus: A general computer code for explicit Lagrangian computation. In: *Proc. 5th Int. Conf. on Structural Integrity In Reactor Technology*, Section B2/8. Berlin, Germany, 1979.

[10] A. Daneri, et al. Influence of the representation models of the stress-strain law on the LMFBR structures in an HCDA. In: *Proc. 6th Int. Conf. on Structural Integrity In Reactor Technology*, Section E4/4. Paris, France, 1981.

[11] F. David. Etude d'une composition explosive flegmatisée. Applications à la déformation d'une cuve. In: *Proc. Symposium sur les hautes pressions dynamiques*. Paris, France, 1978.

[12] C. Fiche, J. Louvet, B.L. Smith, A. Zucchini. Theoretical experimental study of flexible roof effects in an HCDA's simulation. In: *Proc. 8th Int. Conf. on Structural Integrity In Reactor Technology*, Section E4/5, 139-144. Brussels, Belgium, 1985.

[13] A. Hoffmann, M. Lepareux, B. Schwab, H. Bung. Plexus - A general computer program for fast dynamic analysis. In: *Proc. Conf. on Structural Analysis and Design on Nuclear Power Plant*. Porto Alegre, Brazil, 1984.

[14] H. Holtbecker. Testing philosophy and simulation techniques. *Nuclear Engineering and Design*, **42**: 75-87, 1977.

[15] N.E. Hoskin, M.J. Lancefield. The COVA programme for the validation of computer codes for fast reactor containment studies. *Nuclear Engineering and Design*, **46**: 17-46. 1978.

[16] K.C. Kendall, A. Benuzzi. The COVA programme : Validation of the fast reactor containment code SEURBNUK. *Nuclear Engineering and Design*, **57**: 79-105, 1980.

[17] K.C. Kendall, D.J. Adnams. Experiments to validate structural dynamics code used in fast reactor safety assessment. *Science and Technology of Fast Reactor Safety*, Vol. 2. British Nuclear Energy Society, London, England, 1986.

[18] M. Lepareux, B. Schwab, A. Hoffmann, P. Jamet, H. Bung. Un programme général pour l'analyse dynamique rapide - Cas des tuyauteries. In: *Proc. Colloque Tendances Actuelles en Calcul des Structures*. Bastia, France, 1985.

[19] M. Lepareux, B. Schwab, H. Bung. Plexus: A general computer program for the fast dynamic analysis The case of pipe-circuits. In: *Proc. 8th Int. Conf. on Structural Mechanics In Reactor Integrity*, Vol. F1 2/1. Brussels, Belgium, 1985.

[20] M. Lepareux, H. Bung, A. Combescure, J. Aguilar. Analysis of a CDA in a LMFBR with a multiphasic and multicomponent behaviour law. In: *Proc. 11th Int. Conf. on Structural Mechanics In Reactor Integrity*, Section E13/1, 371-376. Tokyo, Japan, 1991.

[21] M. Lepareux, H. Bung, A. Combescure, J. Aguilar, J.F. Flobert. Analysis of an HCDA in a fast reactor with a multiphase and multicomponent behavior law. In: *Proc. 12th Int. Conf. on Structural Mechanics In Reactor Integrity*, Section E7/2, 197-202. Stuttgart, Germany, 1993.

[22] M. Lepareux, J.M. Michelin, D. Thiault. Plexus-R : une extension de Plexus à la robotique. CEA report DMT/94-138, 1994.

[23] J. Louvet, P. Hamon, B.L. Smith, A. Zucchini. MARA 10: an integral model experiment in support of LMFBR containment analysis. In: *Proc. 9th Int. Conf. on Structural Mechanics In Reactor Integrity*, Section E, 331-337. Lausanne, Switzerland, 1987.

[24] J. Louvet. Containment response to a core energy release. Main experimental and theorical issues - Future trends. In: *Proc. 10th Int. Conf. on Structural Mechanics In Reactor Integrity*, Vol. E, 305-310. Anaheim, USA, 1989.

[25] M.F. Robbe, M. Lepareux, H. Bung. Plexus - Notice théorique. CEA report DMT/94-490, 1994.

[26] M.F. Robbe, M. Lepareux, N. Vivien, G. Cénérino. Screening calculations on the vessel lower head behaviour due to an in-vessel steam explosion. In: *Proc. 14th Int. Conf. on Structural Mechanics In Reactor Technology*, Section PW/9. Lyon, France, 1997.

[27] M.F. Robbe, P. Galon, T. Yuritzinn. Castem-Plexus: Un logiciel de dynamique rapide pour évaluer l'intégrité des structures en cas d'accident. In: *Proc. 4th Conf. INSTRUC*. Courbevoie, France, 1999.

[28] M.F. Robbe, M. Lepareux. Scoping calculations of an in-vessel steam explosion. CASTEM-PLEXUS computations. In: *Proc. 8th Int. Conf. On Nuclear Engineering*, paper 8269, CD-rom. Baltimore, USA, 2000.

[29] M.F. Robbe, M. Lepareux. Estimation of the mechanical consequences of an in-vessel steam explosion by means of parametric computations. In: *Proc. 8th International Conference on Numerical Methods in Continuum Mechanics*, CD-rom. Liptovský Ján, Slovak Republic, 2000.

[30] M.F. Robbe, M. Lepareux, C. Trollat. Assessment of the hydrodynamic loads due to a LOCA in a 3-loop PWR. Pipe computations with the code CASTEM-PLEXUS. In : *Proc. 8th Int. Conf. On Numerical Methods in Continuum Mechanics*, Liptovský Ján, Slovak Republic, 2000.

[31] M.F. Robbe, Y. Cariou, M. Lepareux, E. Treille. Numerical simulation of a Hypothetical Core Disruptive Accident in the MARA8 mock-up with the CASTEM-PLEXUS computer code. In : *Proc. Int. Conf. on Numerical Methods in Continuum Mechanics 2000*, CD-rom. Liptovský Ján, Slovak Republic, 2000.

[32] M.F. Robbe, Y. Cariou, M. Lepareux, E. Treille. Validation of the Core Disruptive Accident constitutive law of the Castem-Plexus code on the Mara8 test. In. *Proc. Int. Colloquium in Mechanics of Solids, Fluids, Structures and Interactions*. Nha Trang, Vietnam, 2000.

[33] M.F. Robbe, N. Vivien, M. Valette, E. Berglas. Use of thermalhydraulic and mechanical linked computations to estimate the mechanical consequences of a steam explosion. *Slovak Journal of Mechanical Engineering* 52, Vol. 2, 65-90, 2001.

[34] M.F. Robbe, M. Lepareux, E. Treille, Y. Cariou. Numerical simulation of a Core Disruptive Accident and comparison with the simple test Mara8. In : Proc. ANS/HPS Student Conference " 2001 : A nuclear odyssey ", CD-rom. Texas A&M University, USA, 2001.

[35] M.F. Robbe, M. Lepareux, E. Treille, Y. Cariou. Numerical simulation of an explosion in a simple scale model of a nuclear reactor. *Computer Assisted Mechanics and Engineering Sciences*, to appear.

[36] M.F. ROBBE, M. LEPAREUX. Evaluation of the mechanical consequences of a steam explosion in a nuclear reactor, *Bulgarian Journal of Theoretical and Applied Mechanics*, in press, 2002.

[37] M.F. Robbe, M. Lepareux, C. Trollat. Hydrodynamic loads on a PWR primary circuit due to a LOCA. *Nuclear Engineering and Design*, in press, 2002.

[38] J.E.A. Sidoli, K.C. Kendall. The WINCON programme - Validation of the fast reactor primary containment codes. In: D.G. Walton, *Proc. INE Int. Conf. On Nuclear Containment*. Nuclear Containment Structures, Cambridge University Press, 1988.

[39] B.L. Smith, C. Fiche, J. Louvet, A. Zucchini. A code comparison exercise based on the LMFBR containment experiment MARA-04. In : *Proc. 8th Int. Conf. on Structural Mechanics In Reactor Technology*, Section E4/7, 151-157. Brussels, Belgium, 1985.

[40] E. Struder, P. Galon. Hydrogen combustion loads Plexus calculations. *Nuclear Engineering and Design*, **174**: 119-134, 1997.

[41] H.U. Wenger, B.L. Smith. On the origin of the discrepancies between theory and experiment in the COVA series. In: *Proc. 9th Int. Conf. on Structural Mechanics In Reactor Technology*, Vol. E, 339-344. Lausanne, Switzerland, 1987.

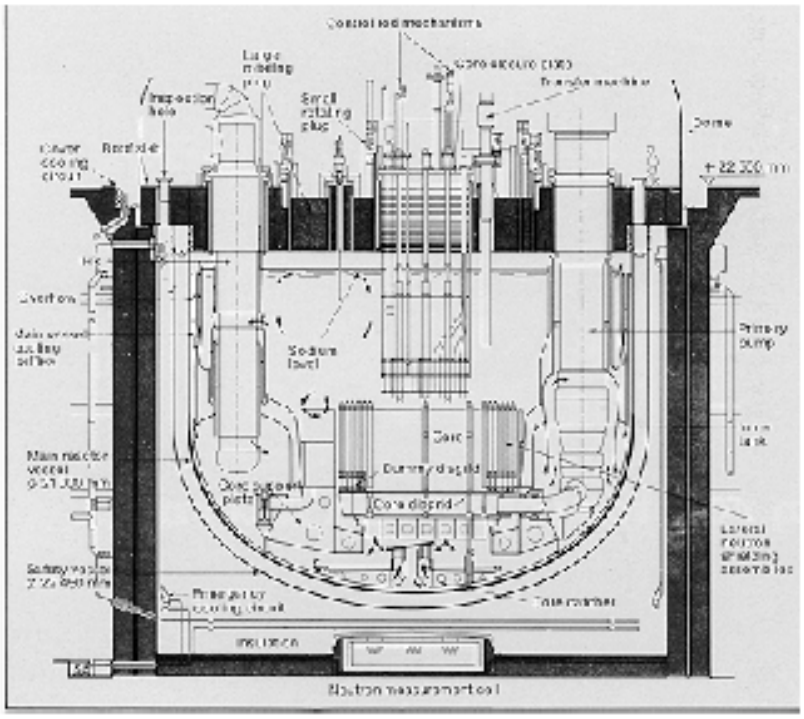

Fig. 1: The Superphenix reactor

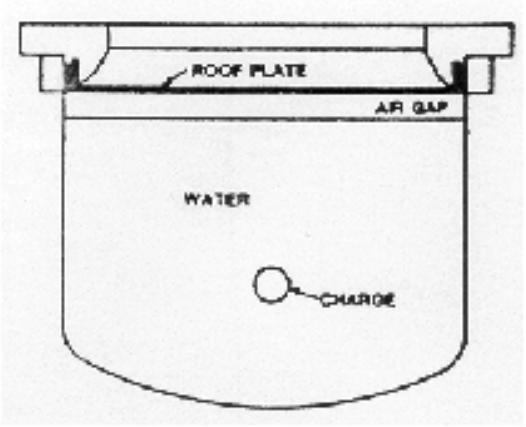

Fig. 2: The MARA8 mock-up

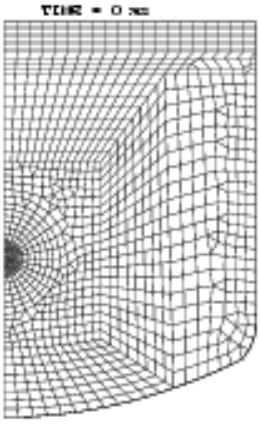

Fig. 3: Mesh of the MARA8 test

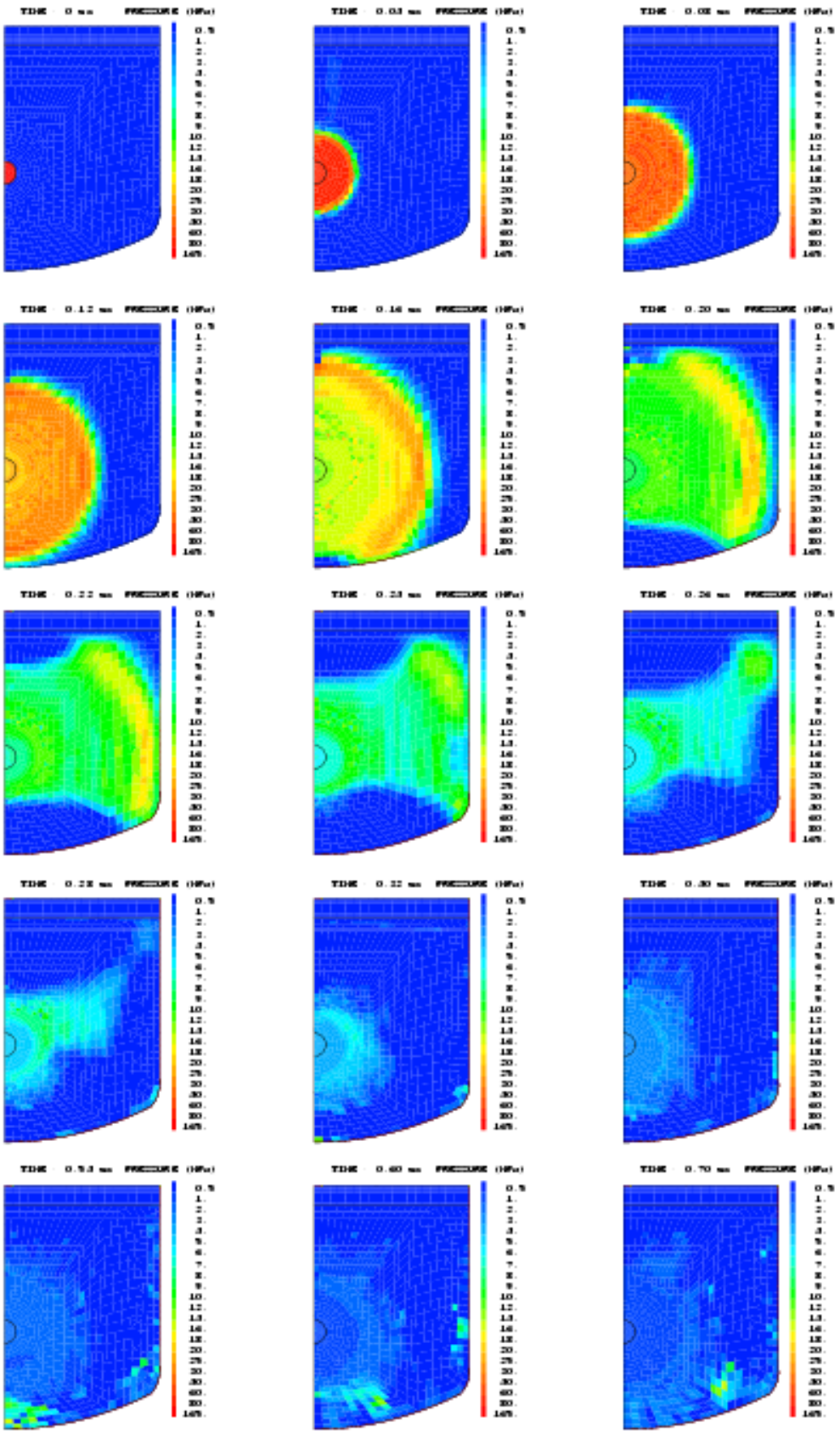

Fig. 4: Pressure

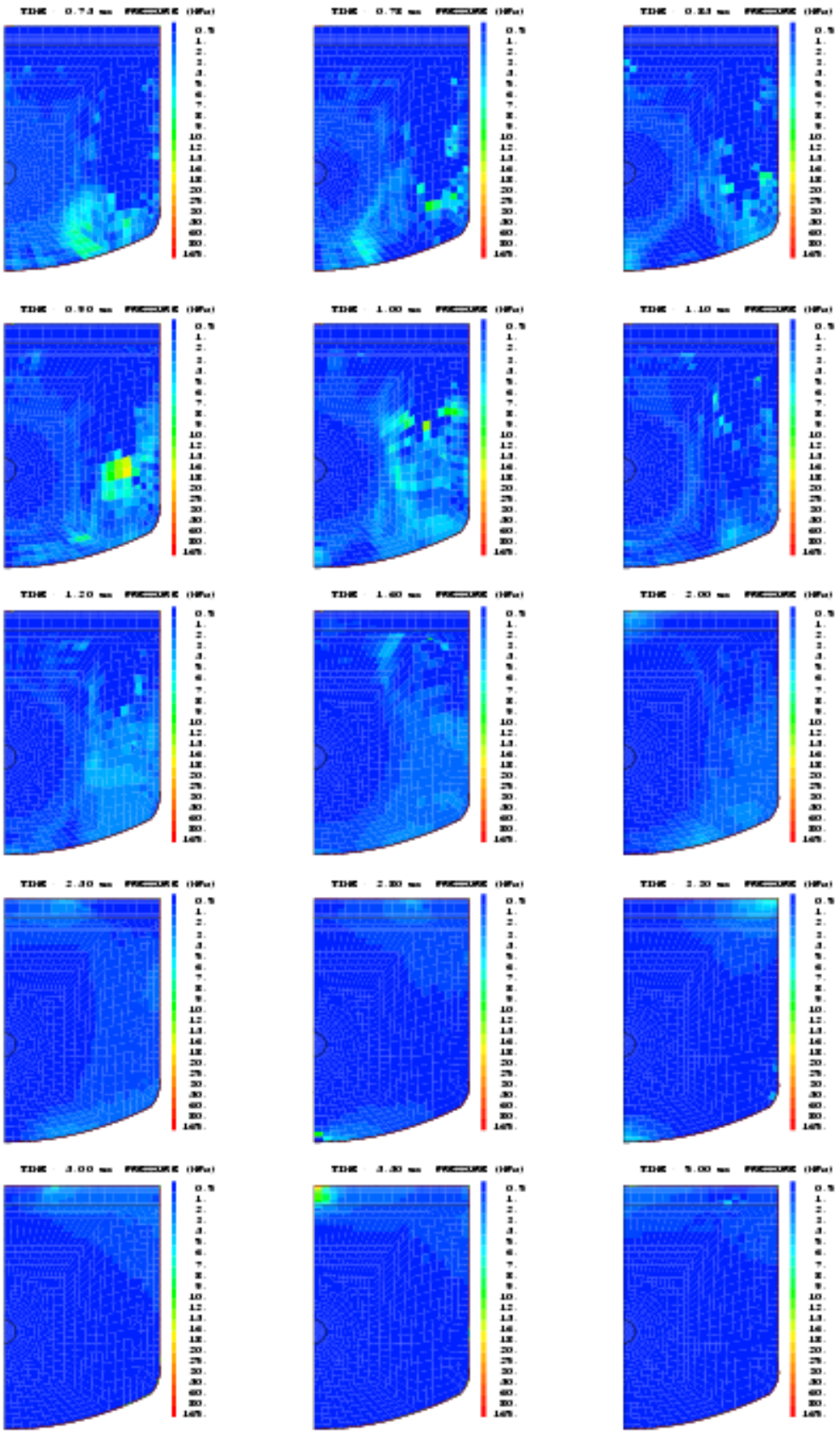

Fig. 4: Pressure

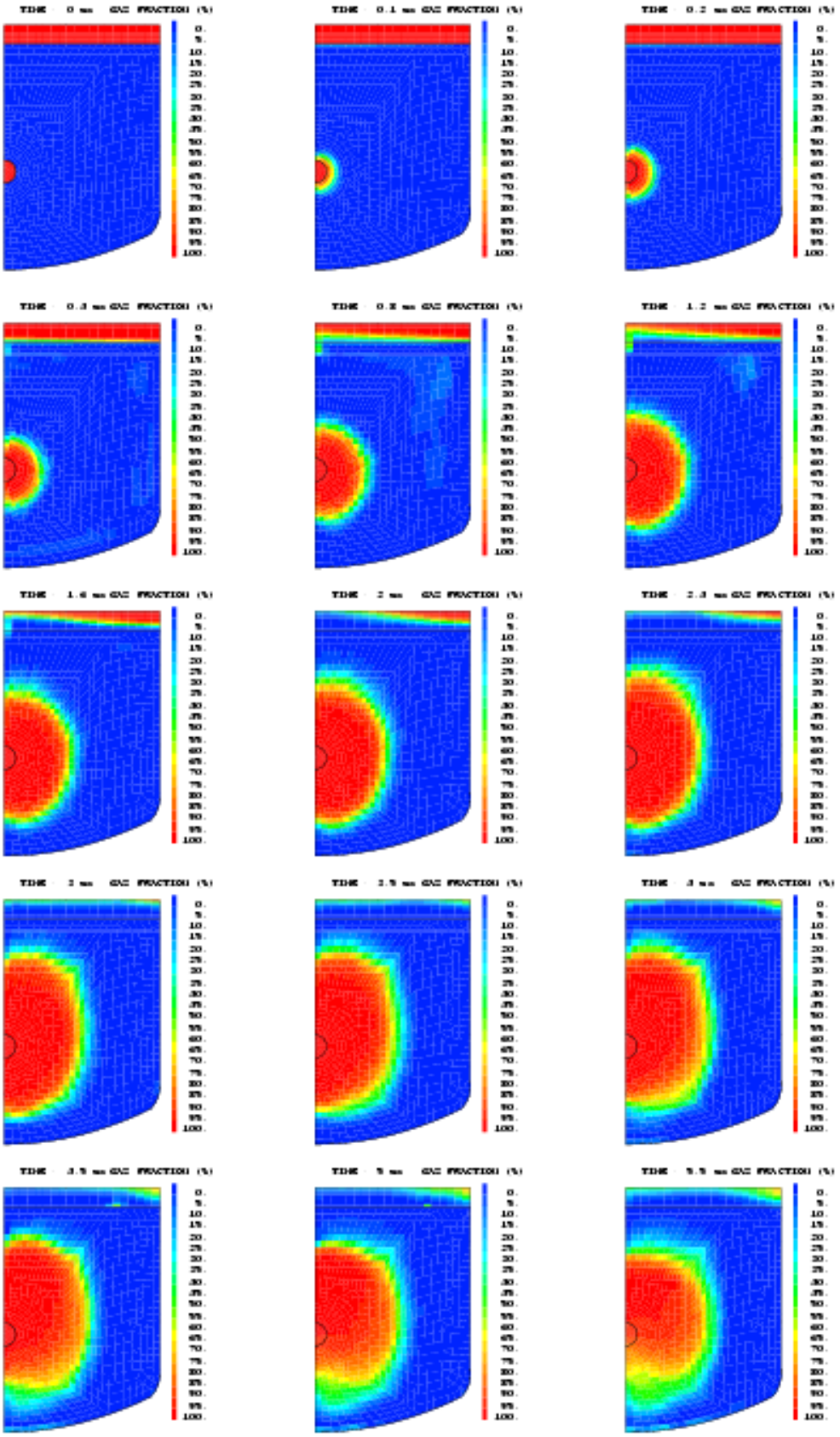

Fig. 5: Volumic presence fraction of gas

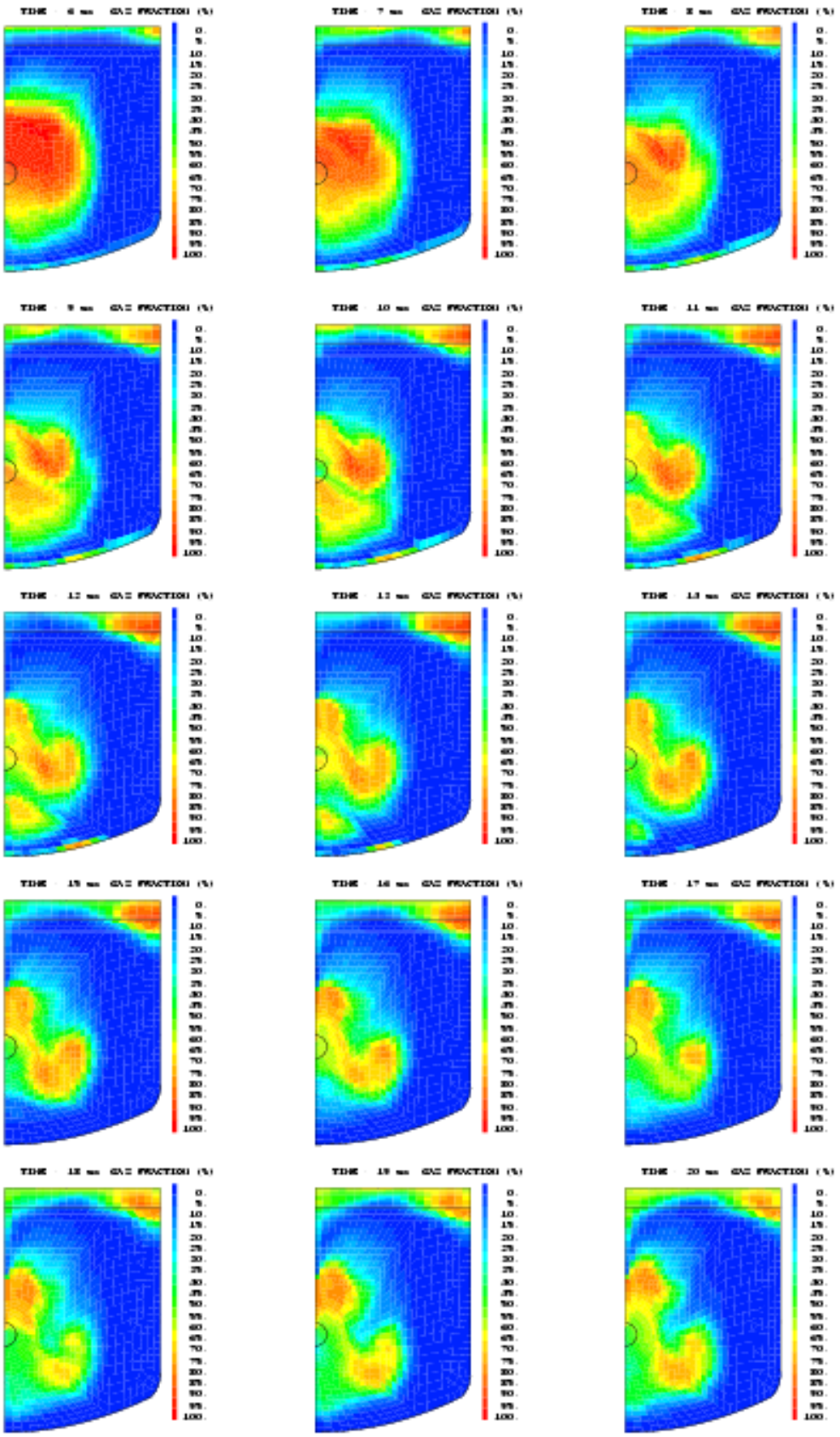

Fig. 5: Volumic presence fraction of gas

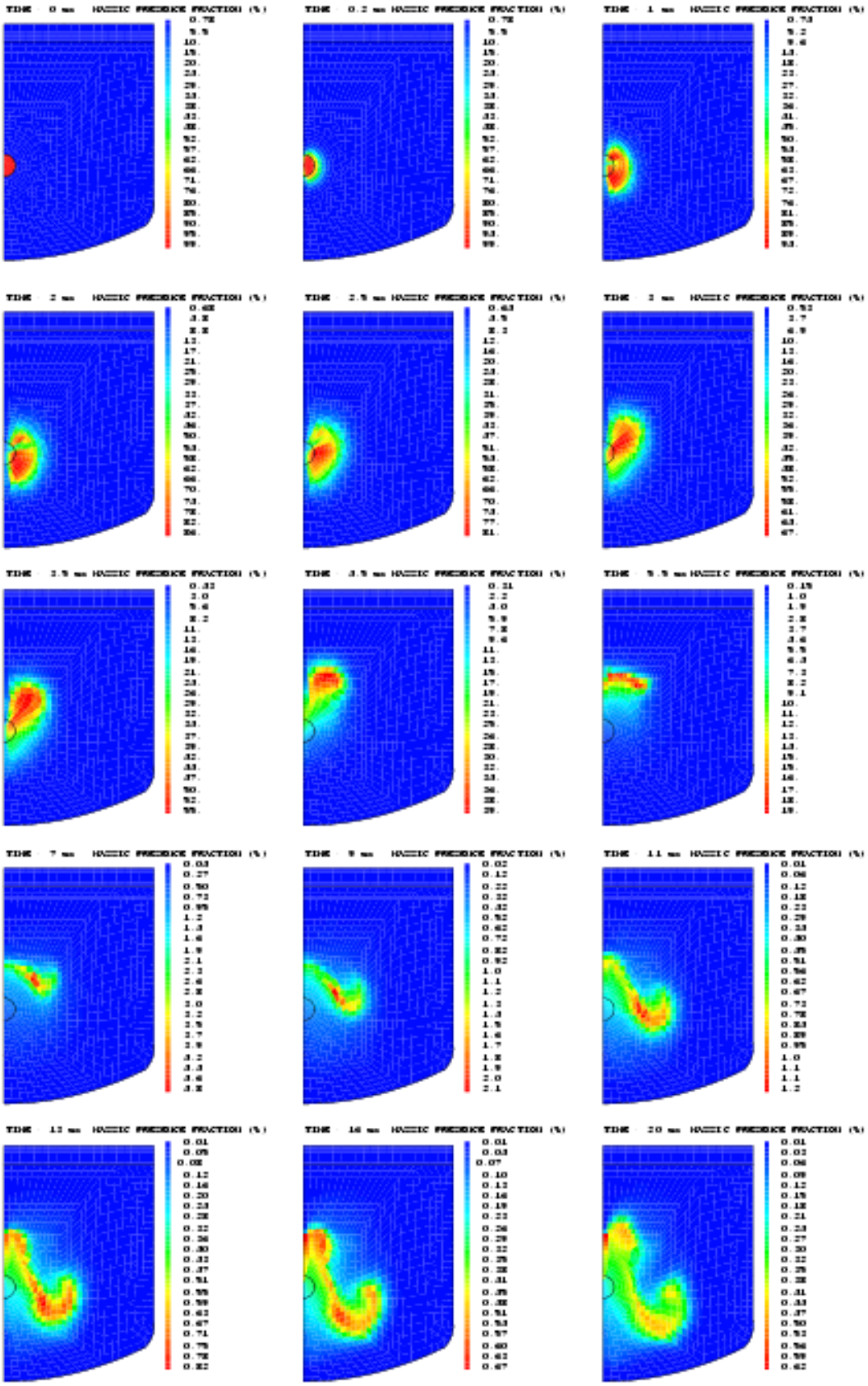

Fig. 6: Massic presence fraction of the bubble

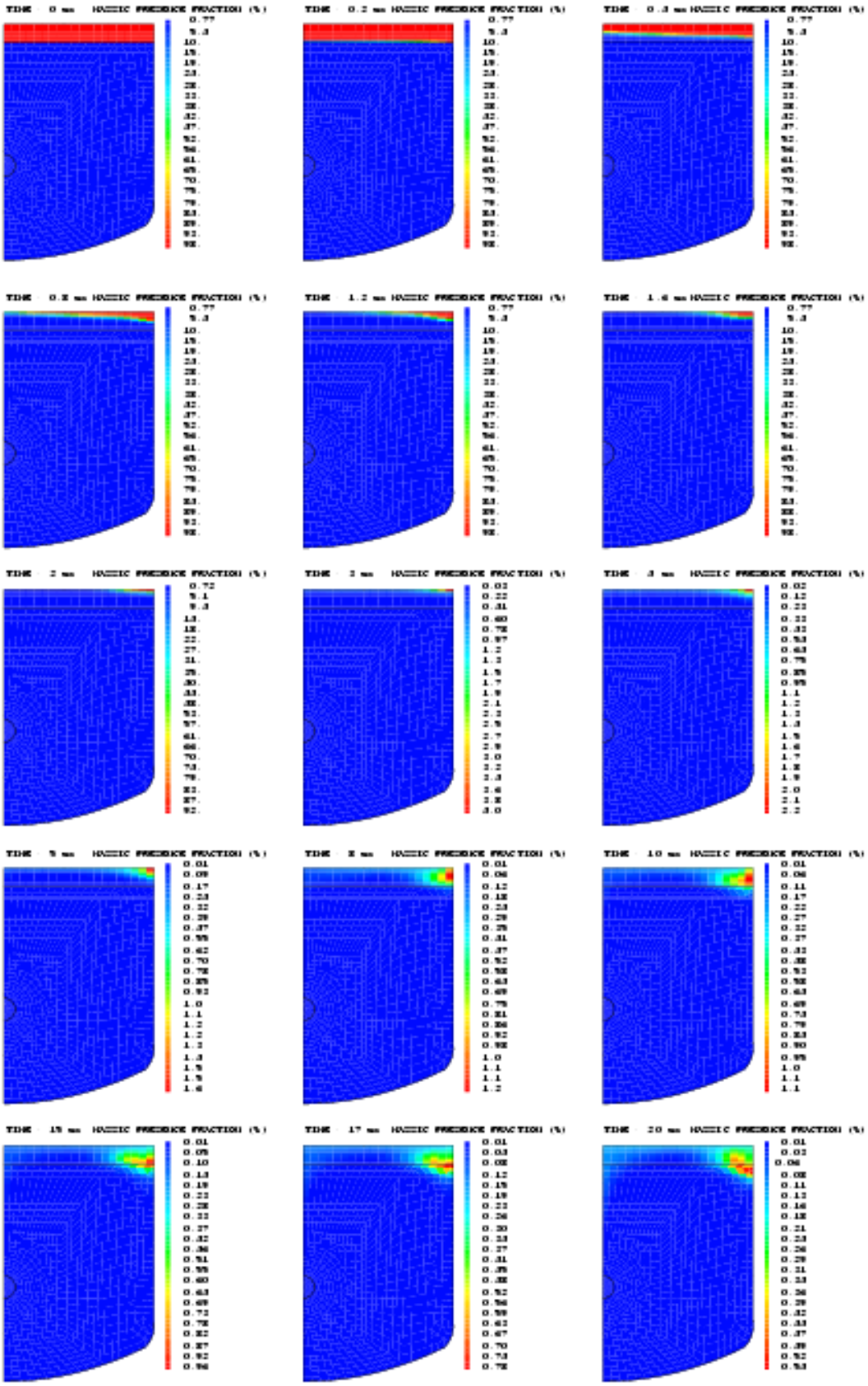

Fig. 7: Massic presence fraction of air

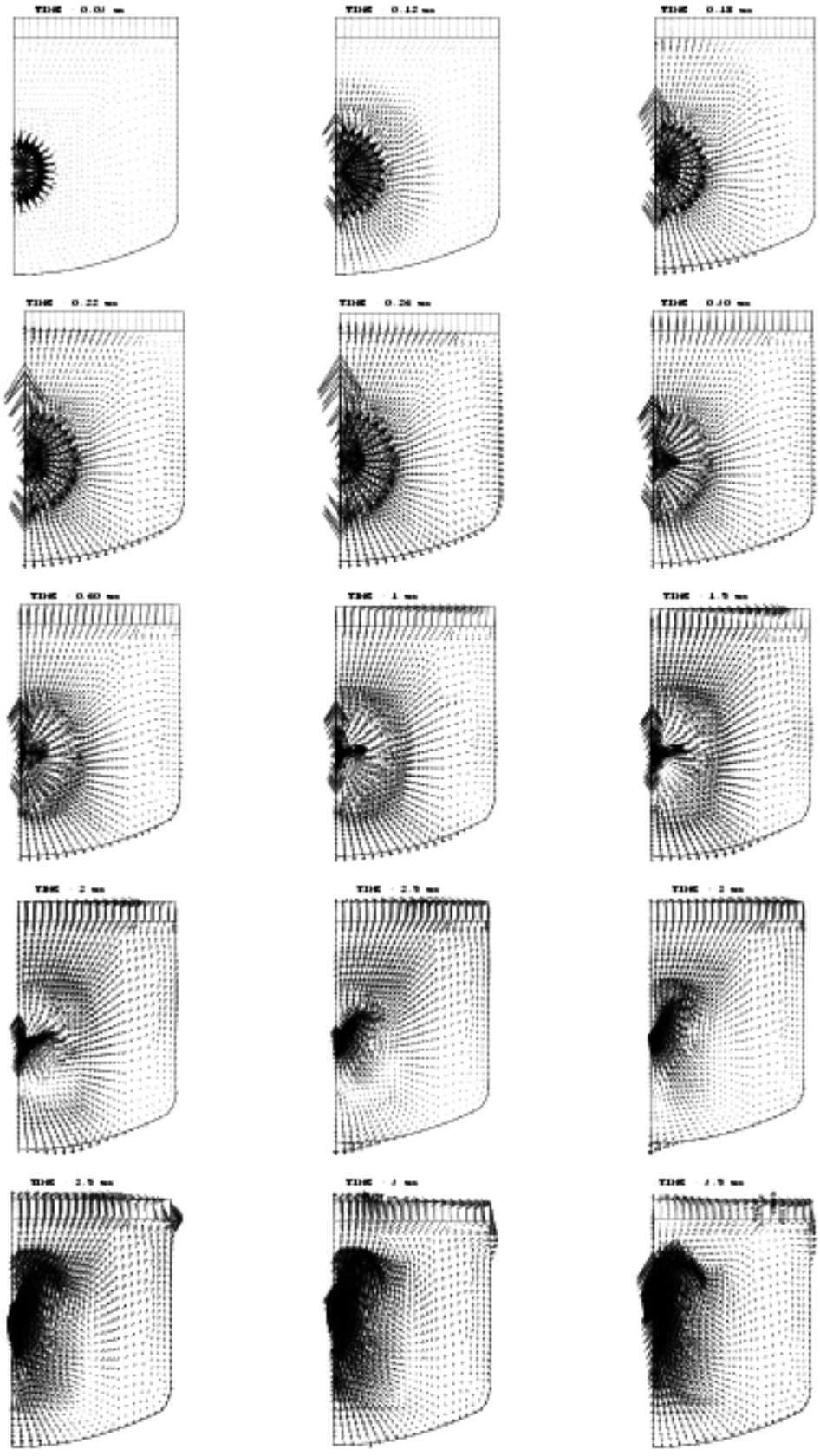

Fig. 8: Fluid speed

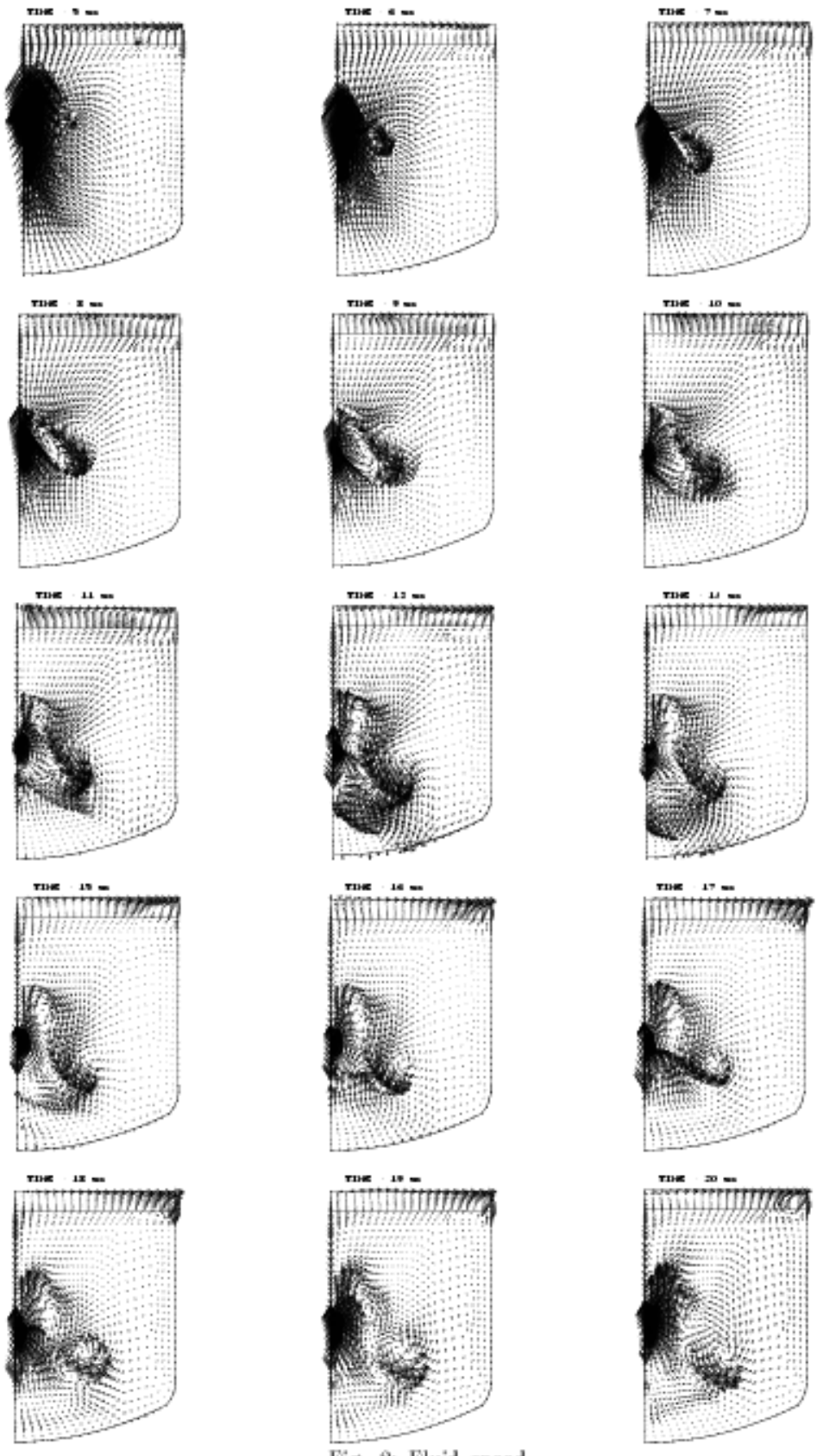

Fig. 8: Fluid speed

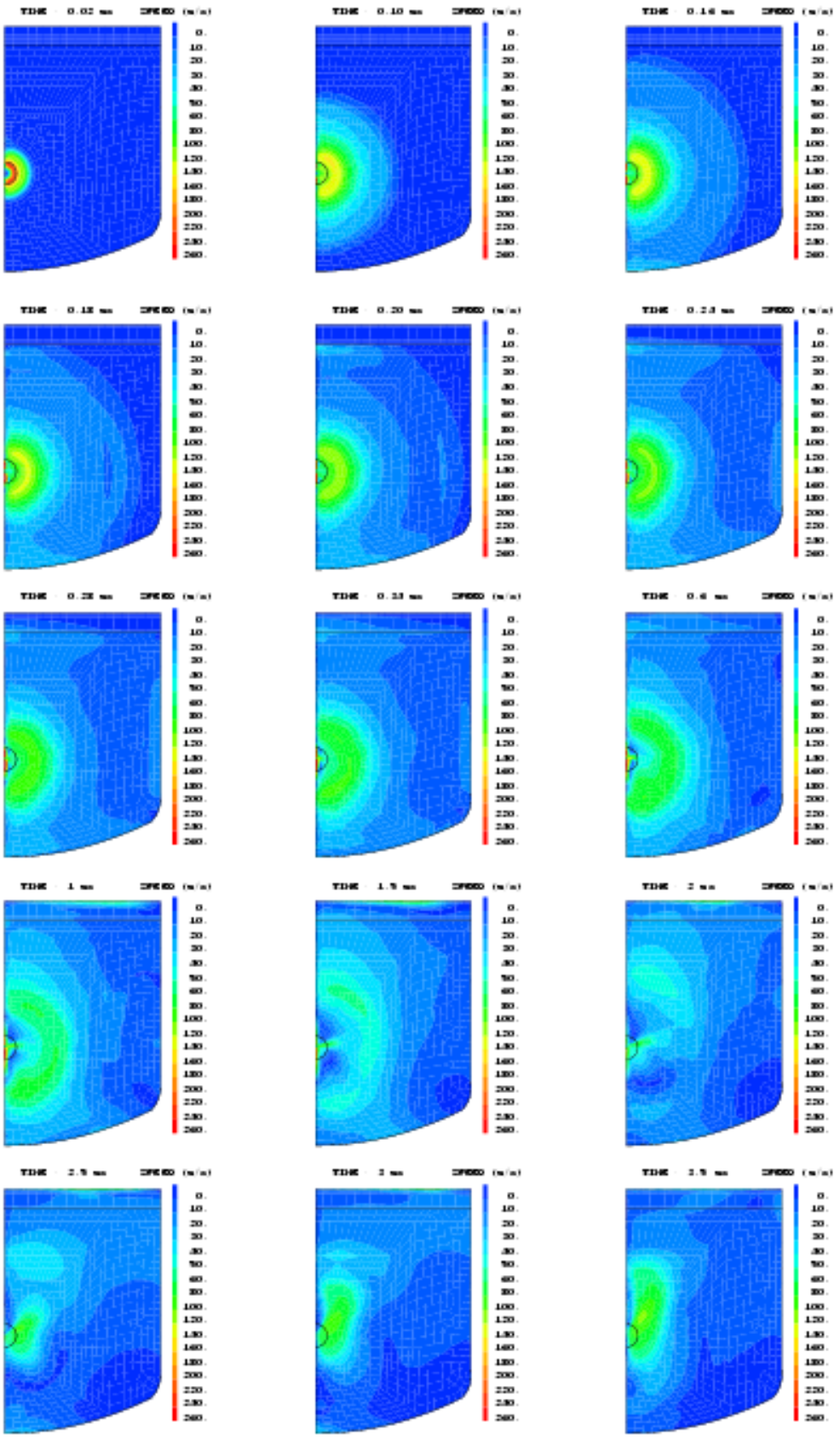

Fig. 9: Fluid speed

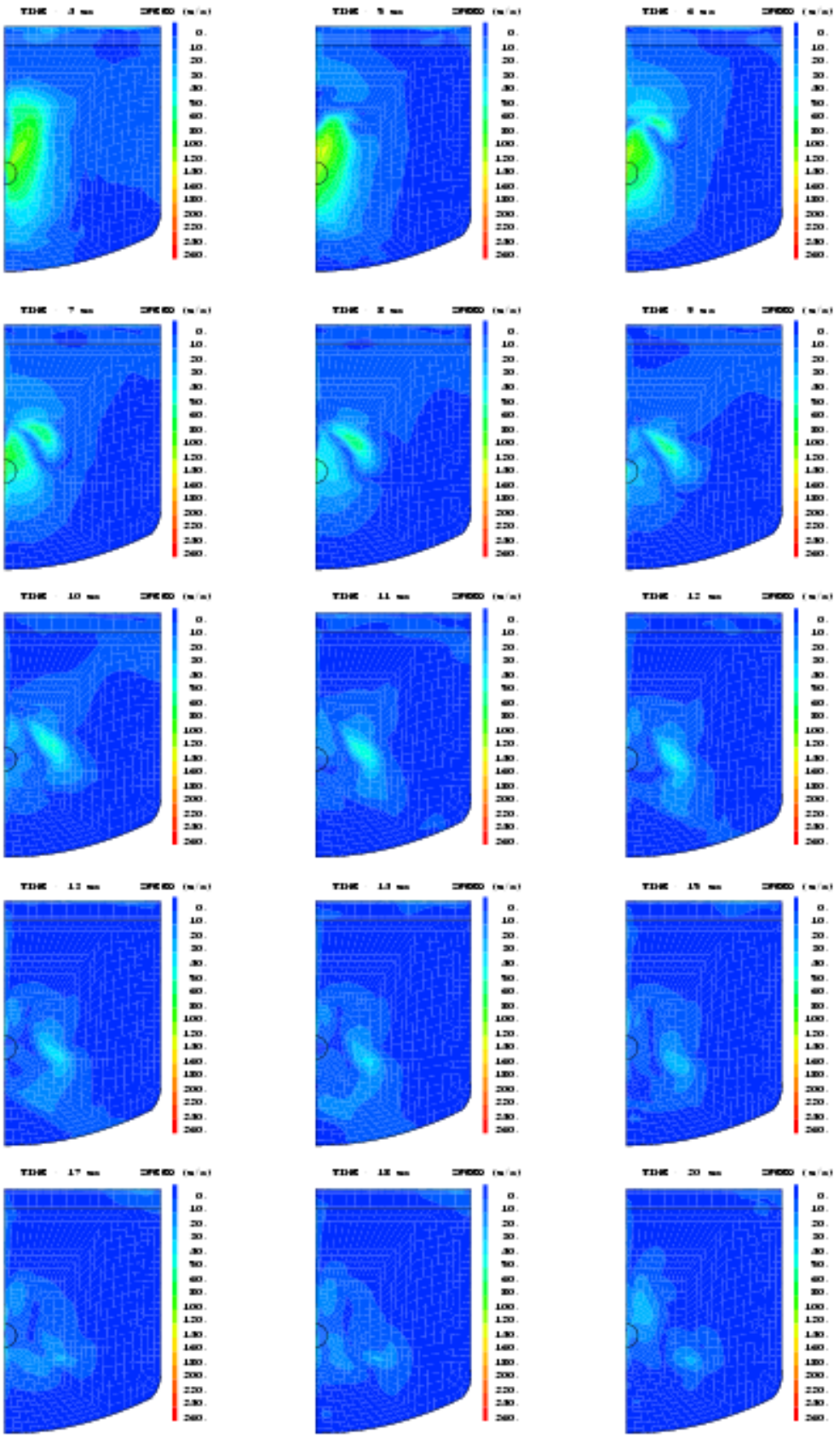

Fig. 9: Fluid speed

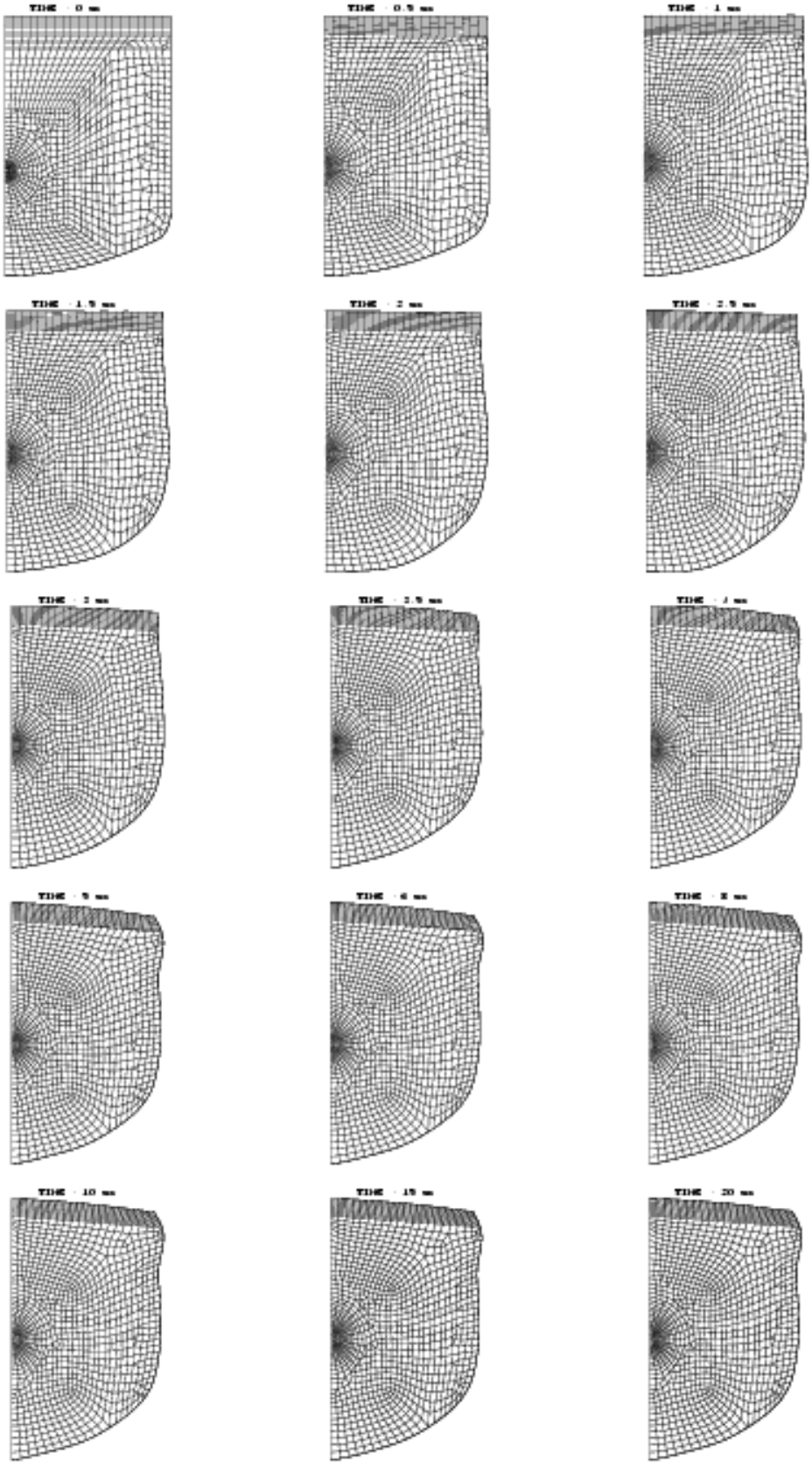

Fig. 10: Deformed shape

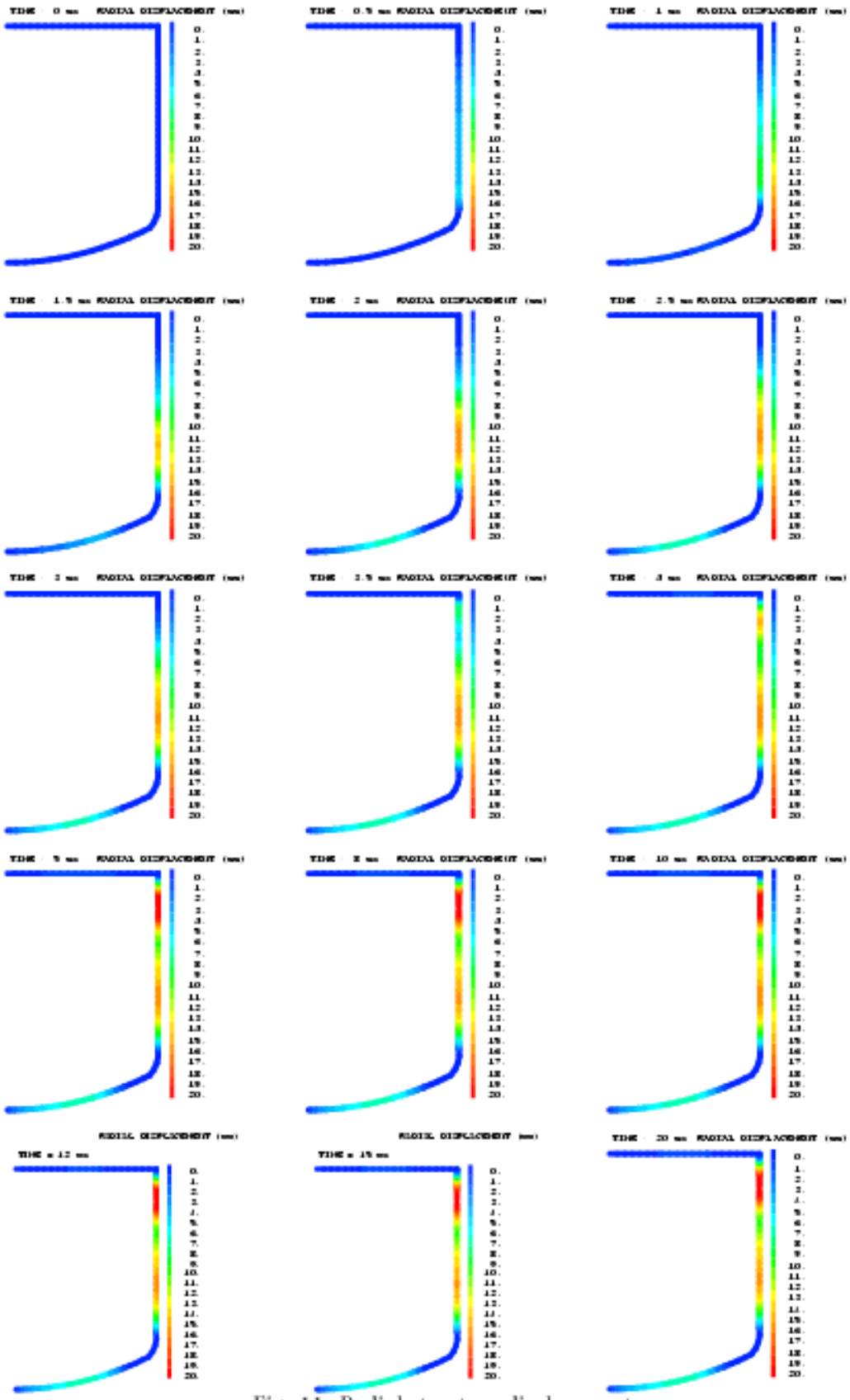

Fig. 11: Radial structure displacements

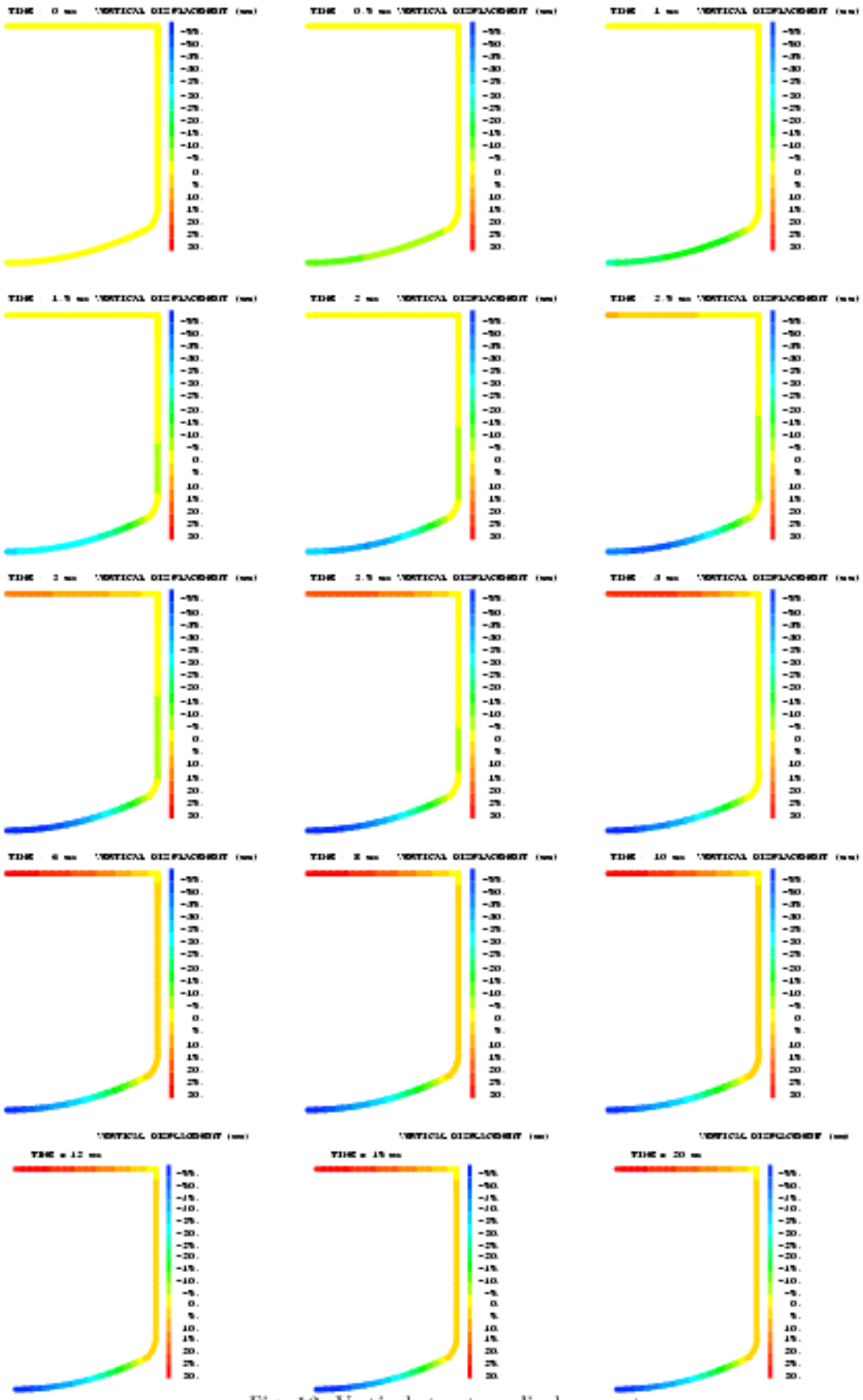

Fig. 12: Vertical structure displacements

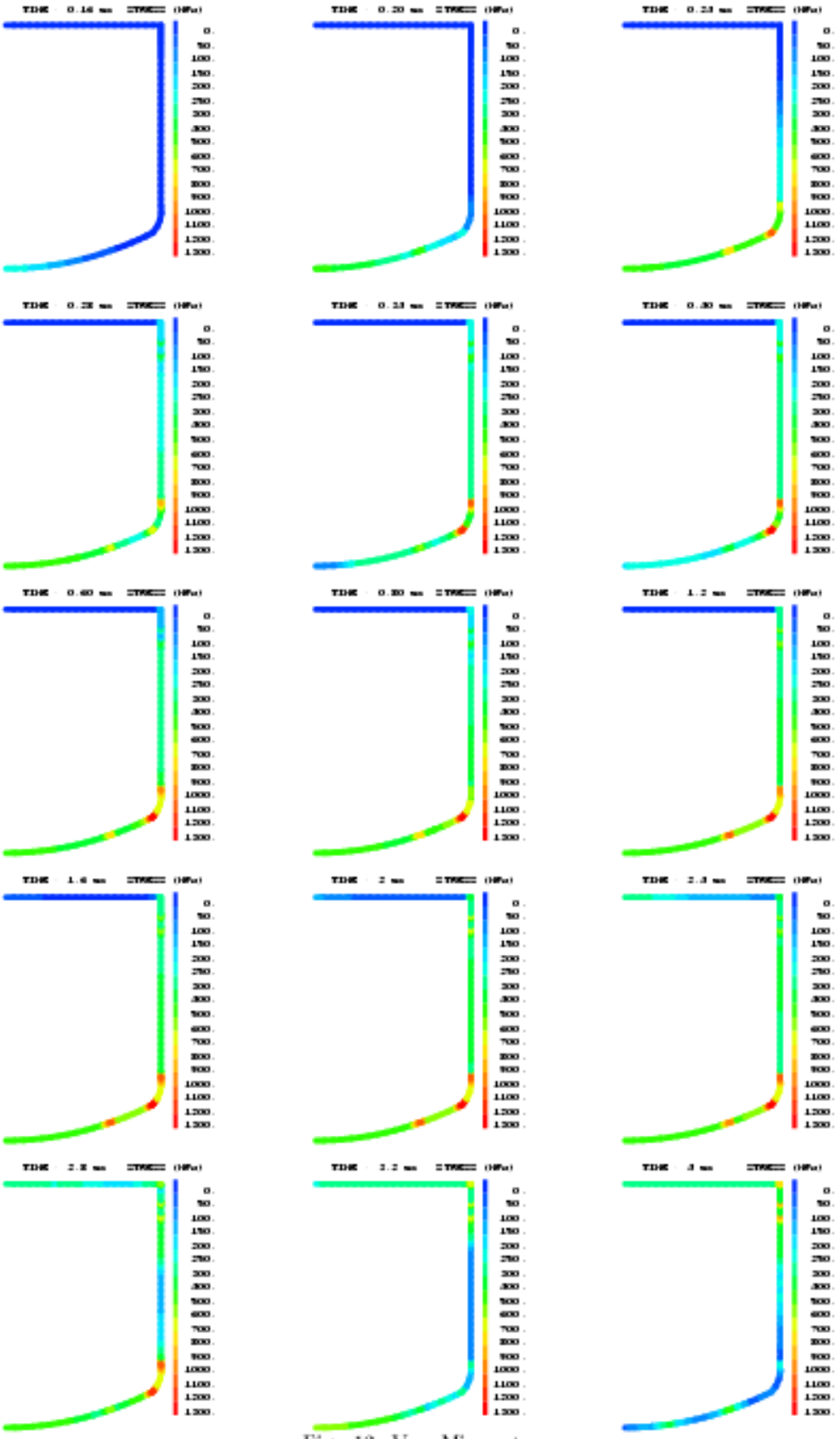

Fig. 13: Von Mises stresses

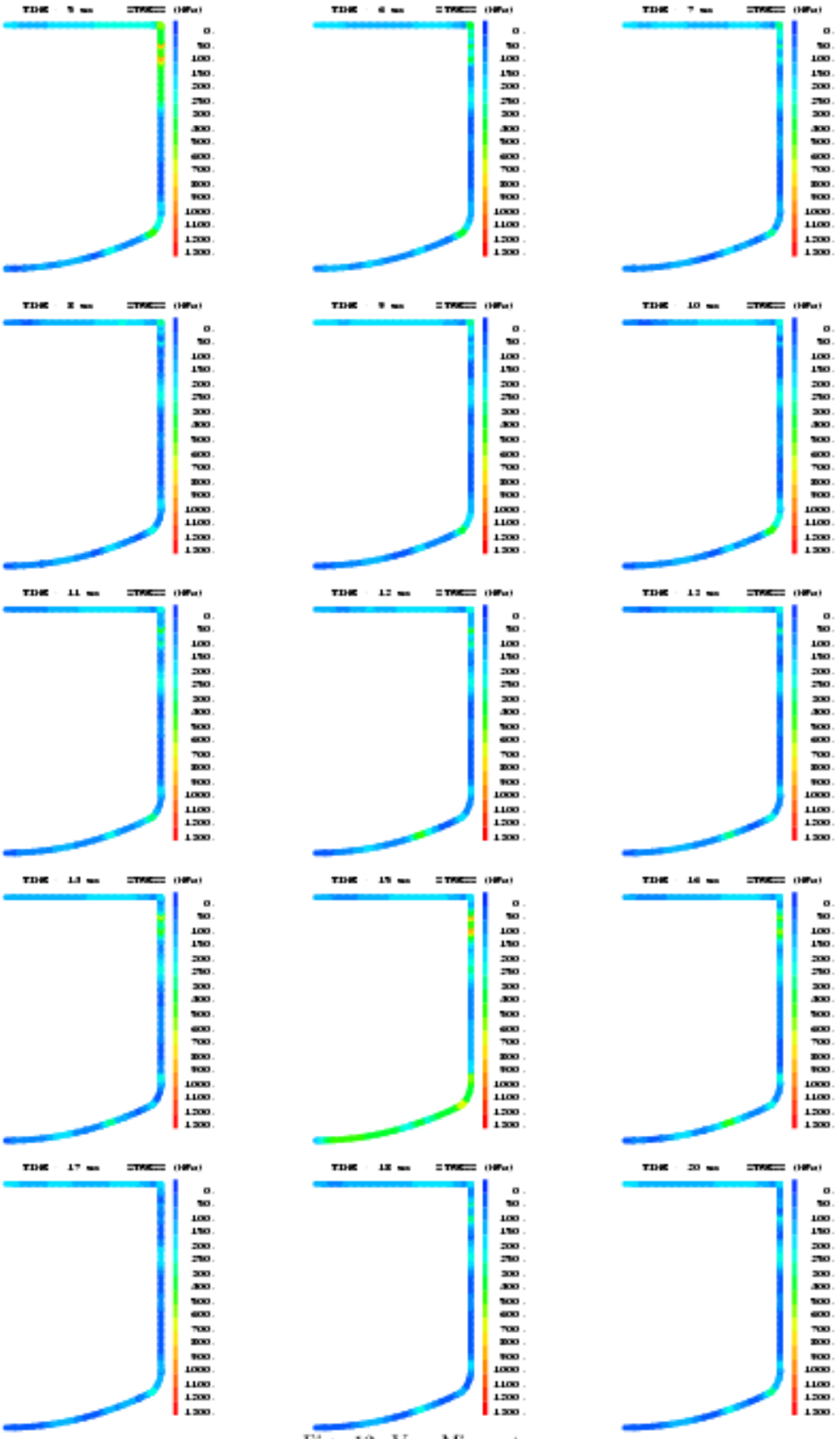

Fig. 13: Von Mises stresses

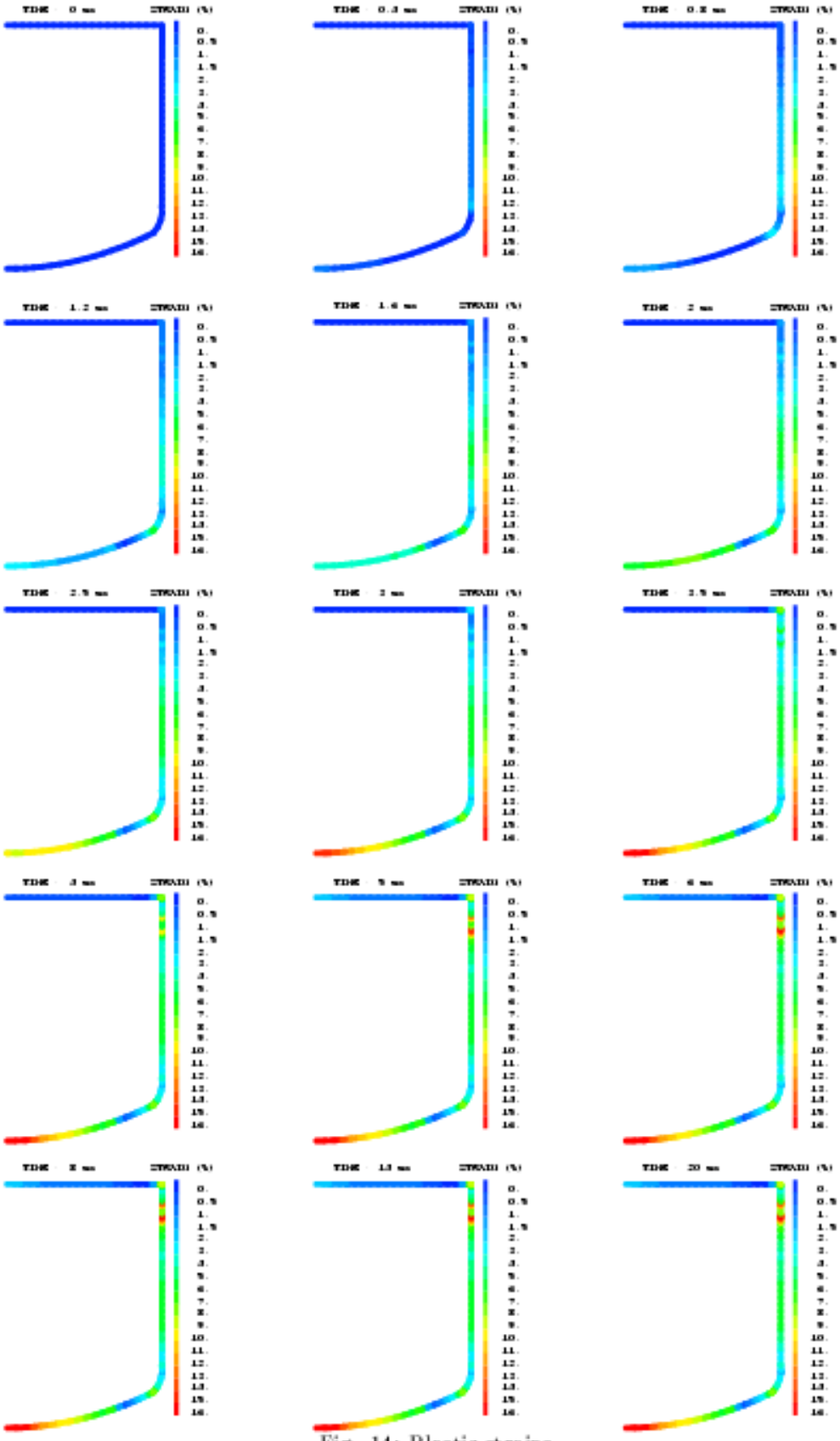

Fig. 14: Plastic strains

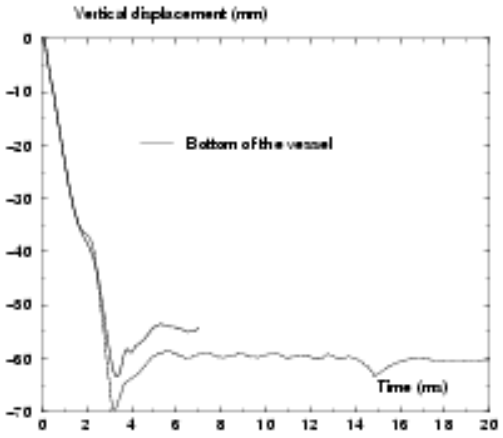

Fig. 15: Vertical displacement at the bottom of the vessel

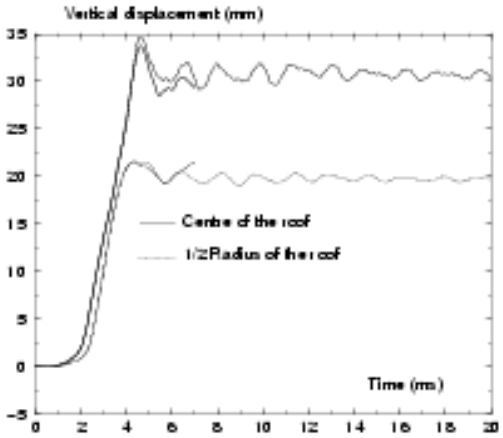

Fig. 16: Vertical displacement of the roof

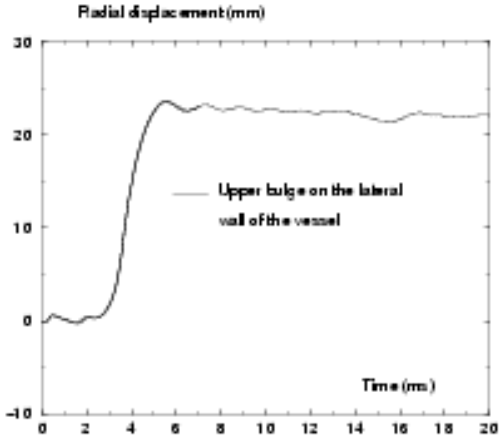

Fig. 17: Radial displacement on the upper bulge (lateral wall of the vessel)

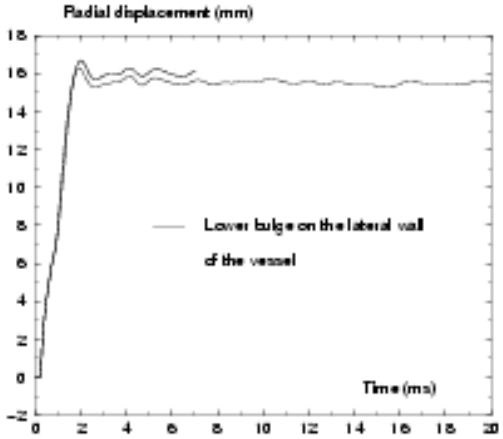

Fig. 18: Radial displacement on the lower bulge (lateral wall of the vessel)

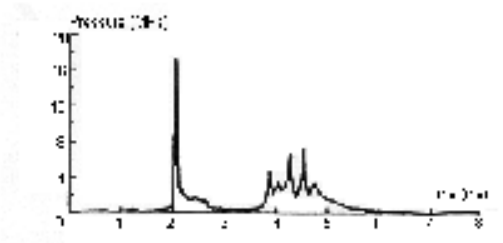

Fig. 19: Experimental pressure

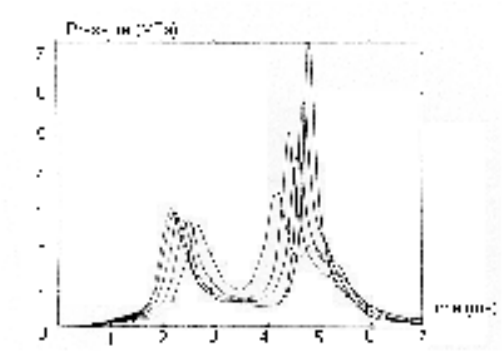

Fig. 20: Pressure under the roof, computed by CASTEM-PLEXUS

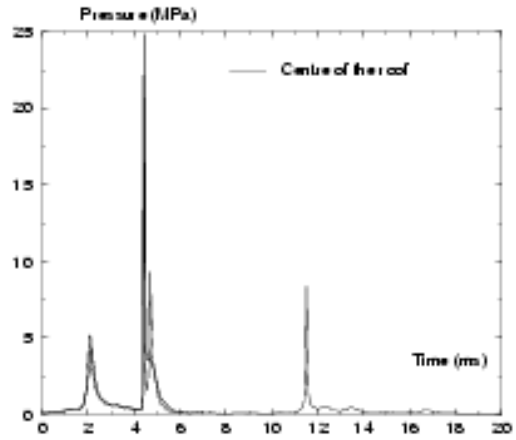

Fig. 21: Pressure under the roof (in the centre)

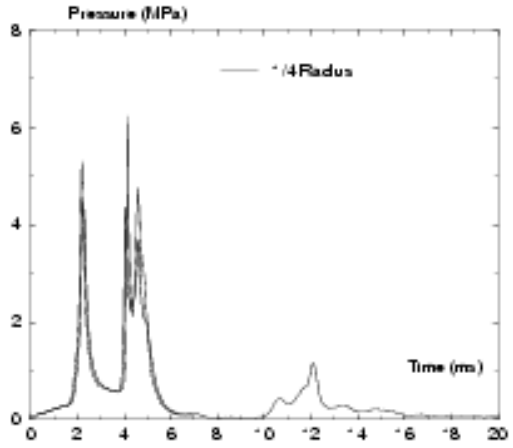

Fig. 22: Pressure under the roof (1/4 of the radius)

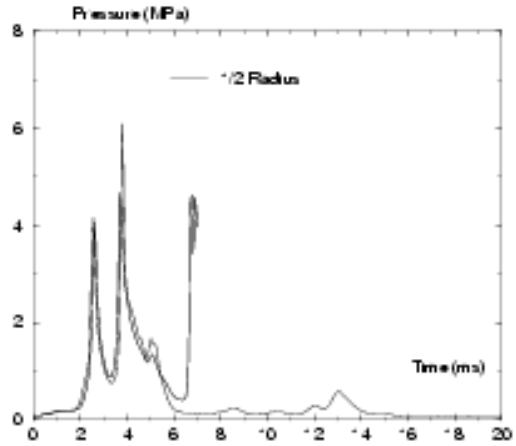

Fig. 23: Pressure under the roof (mid-radius)

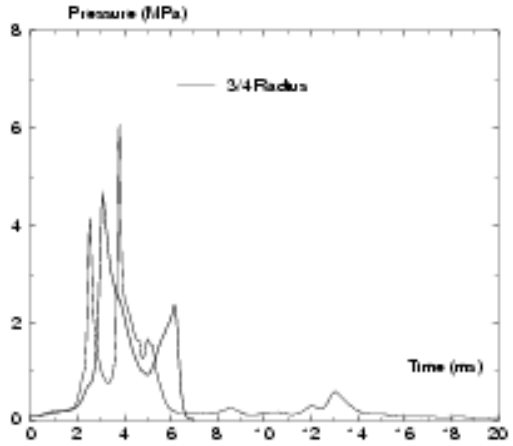

Fig. 24: Pressure under the roof (3/4 of the radius)

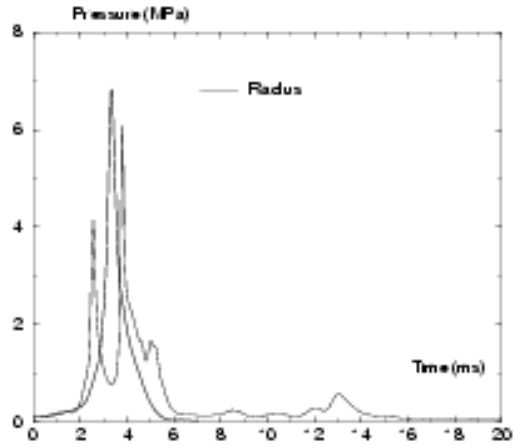

Fig. 25: Pressure under the roof (near the vessel)

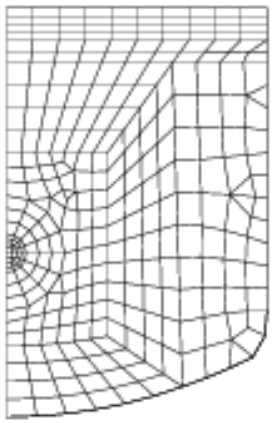

Fig. 26: Mesh of the old CASTEM-PLEXUS calculations

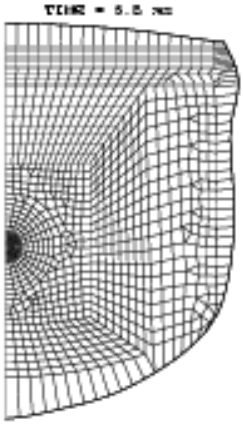

Fig. 27: Deformed mesh at the end of the previous EUROPLEXUS simulation

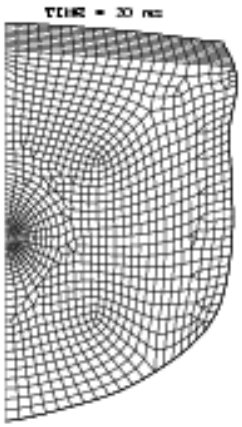

Fig. 28: Deformed mesh at the end of the current EUROPLEXUS simulation

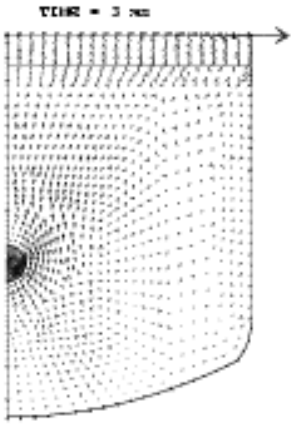

Fig. 29: Flows at 3 ms for the previous EUROPLEXUS simulation

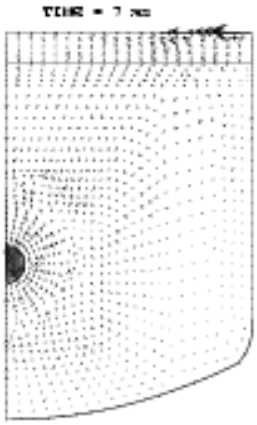

Fig. 30: Flows at 7 ms for the previous EUROPLEXUS simulation

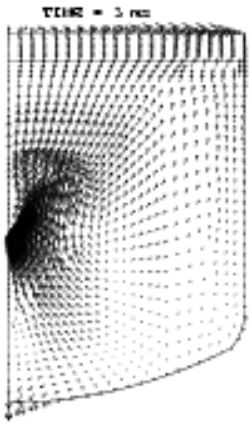

Fig. 31: Flows at 3 ms for the current EUROPLEXUS simulation

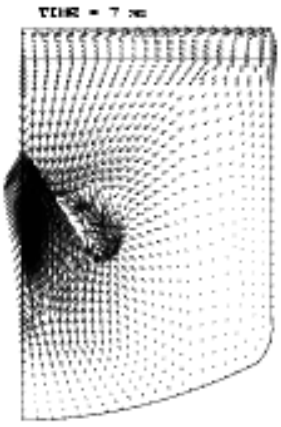

Fig. 32: Flows at 7 ms for the current EUROPLEXUS simulation

		Experiment		SIRIUS computations		CP computations		EP1 computations		EP2 computations	
		Maximum	Final	Maximum	Final	Maximum	Final	Maximum	Final	Maximum	Final
Bottom of the vessel	Vert. displacement (cm)	5.5	5.2	5.4		6.5	5.7	6.3	5.4	7.0	6.0
	Instant of max (ms)	2.75		2.6		3.5		3.3		3.2	
Upper bulge of the vessel	Hoop strain (%)	5.4	4.6	3.8		6.0	5.5	6.7	6.5	6.7	6.3
	Instant of max (ms)	5.0		5.1		5.3		5.6		5.5	
	Distance to the roof (cm)		4.8		5.0		7.3		6.7		6.0
Lower bulge of the vessel	Hoop strain (%)	5.0	4.2	4.1		4.7	4.4	4.8	4.6	4.7	4.4
	Instant of max (ms)	1.7		1.7		2.0		2.0		2.0	
Roof	Vert. displacement at the centre (cm)	3.8	2.8	3.6		3.0	2.6	3.4	2.9	3.5	3.1
	Vert. displacement at mid-radius (cm)	2.4	1.9	2.3		2.0	1.8	2.2	2.2	2.2	2.0
	Instant of max (ms)	4.5		4.4		4.6		4.5		4.6	
Pressure under the roof		1^{st} impact	2^{nd} impact	1^{st} impact	2^{nd} impact	1^{st} impact	2^{nd} impact	1^{st} impact	2^{nd} impact	1^{st} impact	2^{nd} impact
	Max. pressure (MPa)	18.0	7.2			3.0	8.0	centre: 4.0 else: 7.0	centre: 2.5 else5.0	centre: 5.2 else: 4 to 5.5	centre: 2.2 else: 6.2
	Instant of max (ms)	2.1	4 to 5			2.2	4 to 5	2.1	3.5 to 6	2.3	3.7 to 5.5

Table 1: Comparison between the experimental results and the results computed by SIRIUS, CASTEM-PLEXUS and EUROPLEXUS